Lithos 380–381 (2021) 105853

Contents lists available at ScienceDirect

Lithos

journal homepage: www.elsevier.com/locate/lithos

Research Article

Geochemical and geochronological record of the Andaman Ophiolite, SE Asia: From back-arc to forearc during subduction polarity reversal?

Debaditya Bandyopadhyay [a,b,*], Biswajit Ghosh [a], Carl Guilmette [c], Alexis Plunder [d,e], Fernando Corfu [f], Eldert L. Advokaat [d,g], Pinaki C. Bandopadhyay [a], Douwe J.J. van Hinsbergen [d]

[a] Department of Geology, University of Calcutta, 35 Ballygunge Circular Road, Kolkata 700019, India
[b] Department of Geology, University of North Bengal, Darjeeling 734013, India
[c] Département de Géologie et de Génie Géologique, Université Laval, Québec, Québec, Canada
[d] Department of Earth Sciences, Utrecht University, Princetonlaan 8A, 3584, CB, Utrecht, the Netherlands
[e] BRGM, 3 Avenue Claude Guillemin, BP 306009, 45060, Orléans Cedex 2, France
[f] Department of Geosciences and CEED, University of Oslo, Oslo, Norway
[g] School of Geography, Earth and Environmental Sciences, University of Birmingham, Birmingham B15 2TT, United Kingdom

ARTICLE INFO

Article history:
Received 8 June 2020
Received in revised form 25 September 2020
Accepted 17 October 2020
Available online 22 October 2020

Keywords:
Andaman Ophiolite
Agglomerate
Plagiogranite
U-Pb Zircon age
Tectonic discrimination
Subduction initiation

ABSTRACT

Ophiolites are widely studied to unravel how new subduction zones form. They may contain crustal and mantle rocks that formed during juvenile stages of intra-oceanic subduction, modifying the pre-existing oceanic lithosphere within which subduction started, and in which a magmatic arc formed upon subduction maturation. Previous geochemical work on the Cretaceous Andaman Ophiolite and its metamorphic sole, located in the forearc of the Sunda subduction zone of south-east Asia, has revealed geochemical signatures that are difficult to reconcile in a single tectonic setting but may rather record different stages in a longer evolution. A recent kinematic reconstruction proposed that the Andaman Ophiolite may have formed during subduction initiation in a former back-arc basin, when the former (Woyla) arc collided with the Sundaland continent. Here, we evaluate whether such a scenario may provide a feasible context to explain the enigmatic geochemical signatures preserved in the Andaman Ophiolite. To this end, we provide new, and review existing geochemical as well as geochronological constraints on the formation of its crustal rocks, as well as the evolution of its mantle portion. We identify mafic magmatic rocks and cogenetic plagiogranites that are consistent with formation in a magmatic arc, whereas other magmatic rocks, as well as metamorphic sole protoliths, have characteristics indicative of a back-arc origin. Three new, and two previous zircon U/Pb ages of arc magmatic rocks give a 99–93 Ma age range, but we also identify an inherited ~105 Ma age. This latter age coincides with Ar/Ar cooling ages of the Andaman metamorphic sole, and with a plagioclase xenocryst age from recent Barren Island volcanics east of Andaman. The geochemical and geochronological constraints of the Andaman ophiolites are straightforwardly explained in the context of the regional kinematic history: (1) The original lithosphere formed in the back-arc basin of the Woyla intra-oceanic arc; (2) Subduction initiation and SSZ ophiolite formation within this basin occurred around or slightly before 105 Ma; (3) This was followed by arc magmatism between 99 and 93 Ma upon subduction maturation.

1. Introduction

Ophiolites, oceanic lithosphere fragments that became uplifted and exposed, normally as a result of underthrusting of (subducting) buoyant continental lithosphere, or due to formation of accretionary prisms (e.g. Dewey, 1976; Wakabayashi and Dilek, 2003), are widely recognized as key geological archive to reconstruct the tectonic evolution of lost oceanic plates and plate boundaries (e.g. Pearce et al., 2003; Reagan et al., 2010; Stern et al., 2012; van Hinsbergen et al., 2015). Extensive geochemical work on modern oceanic settings and ophiolite records has revealed that oceanic crust at mid-ocean ridges, back-arc basins, oceanic plateaus, or forearc setting above subduction zones can be geochemically distinguished (e.g. Dilek and Furnes, 2011, 2014; Pearce, 2008, 2014). Particularly the forearc settings, where so-called 'supra-subduction zone (SSZ) ophiolites' form, are of major interest to the geodynamic community because these are thought to signal juvenile stages of subduction (Pearce et al., 1984;Shervais, 2001 ; Stern and Bloomer, 1992). The majority of ophiolites are of this SSZ type and are conventionally explained as the result of upper plate extension at an incipient subduction zone, leading to synchronous decompression melting of upwelling fertile asthenospheric mantle (Shervais, 2001; Stern

* Corresponding author.
E-mail address: debaditya.b2r@gmail.com (D. Bandyopadhyay).

https://doi.org/10.1016/j.lithos.2020.105853
0024-4937/

and Bloomer, 1992). Typical SSZ ophiolites consist of a sequence starting with mid-ocean ridge basalt (MORB)-like forearc basalts (FAB) (Reagan et al., 2010). Subsequently, devolatilization of the gradually subsiding downgoing plate is inferred to lower the solidus of the mantle wedge, causing higher degrees of melting, and producing evolved arc volcanics (particularly at low melting pressures - boninites), followed by mature arc magmatism (Dilek and Furnes, 2011; Stern et al., 2012; Whattam and Stern, 2011). With this general model, ophiolite stratigraphy has been routinely used as a proxy to reconstruct the mechanism and chronology of subduction initiation that took place in earlier geologic history (e.g. Dilek and Furnes, 2011; Parlak, 2016). But, for ophiolites exposed on the Andaman Islands in the east Indian Ocean there appears to be no single tectonic setting that can explain the observed geochemical results (Bandyopadhyay et al., 2020; Plunder et al., 2020).

Located in the forearc east of the Sunda-Burma subduction zone, between Sumatra and Myanmar, the ophiolite suite of the Andaman-Nicobar Accretionary Ridge can potentially provide insight into subduction initiation in the eastern Neotethyan realm that existed between India, Australia and Eurasia (Fig. 1a, 2). The ophiolites were originally regarded as fragments of subducted Indian plate oceanic lithosphere (Curray, 2005; Curray et al., 1979; Mukhopadhyay and Dasgupta, 1988; Pal et al., 2003) or seamounts thereon (Acharyya, 2007; Acharyya et al., 1990; Sengupta et al., 1990) that were offscraped and accreted to the upper, Eurasian margin. However, Pal (2011) suggested that both accreted Indian plate MORB mantle and original mantle wedge of the SE Asian plate are exposed, overlain by supra-subduction zone (boninitic) lavas and subsequent island arc tholeiitic (IAT) volcanics reflecting arc maturation. The Andaman Ophiolites also have a metamorphic sole (Pal and Bhattacharya, 2010; Plunder et al., 2020), which typically forms during subduction initiation and is commonly found below supra-subduction zone ophiolites (e.g. Agard et al., 2016; Guilmette et al., 2018; Hacker and Gnos, 1997; Soret et al., 2017). U–Pb zircon ages for plagiogranites with island arc geochemical signatures (Jafri et al., 1995) yielded ages of 93.6 ±

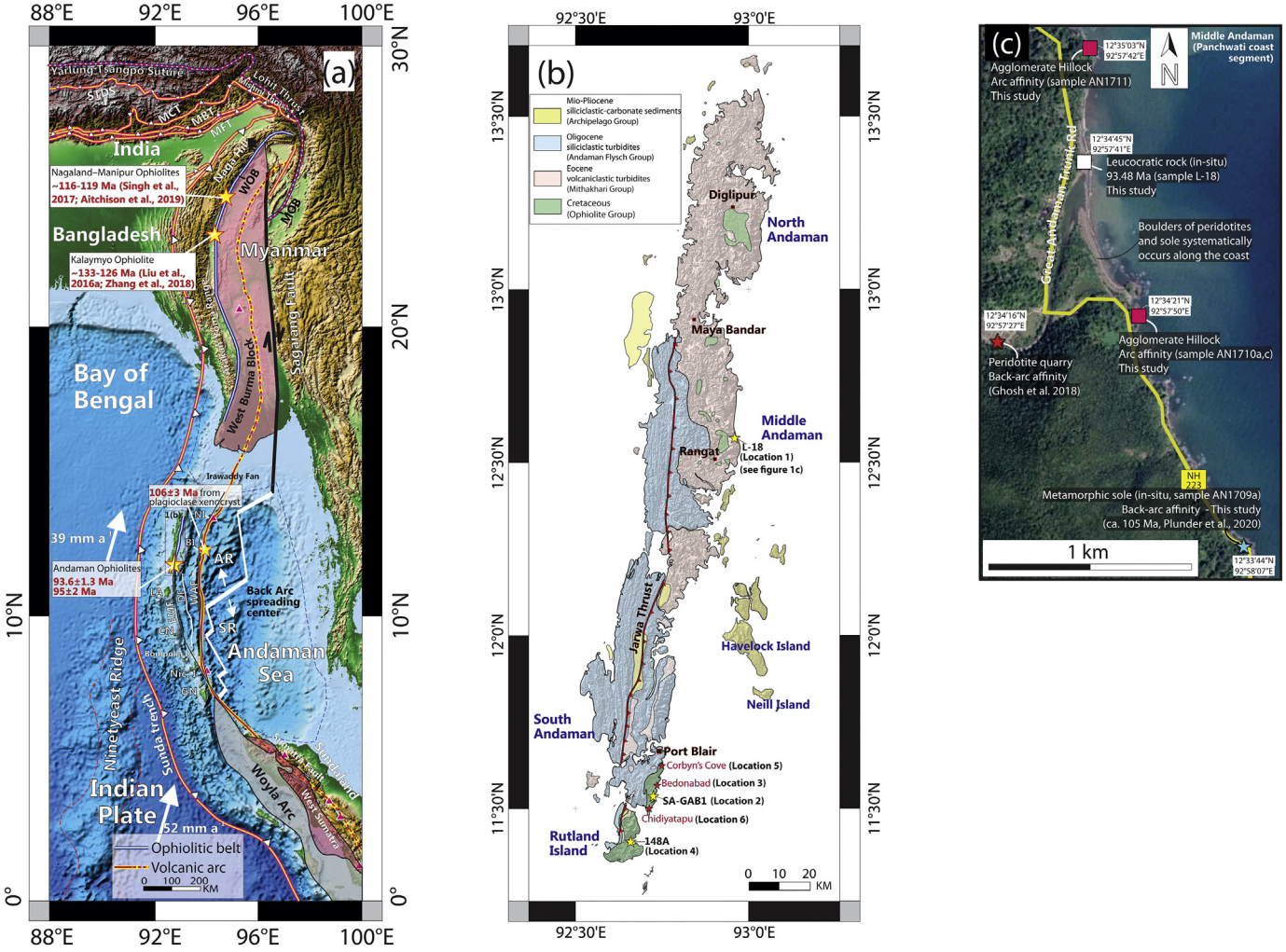

Fig. 1. Tectonic and geological framework of the Andaman ophiolite - (a) Colour-shaded relief image showing the eastern Himalayan syntaxis, the western Burma (Myanmar) region and the Andaman–Sumatra–Java (ASZ) trench in the regional geodynamic framework (modified after Bandyopadhyay et al., 2020). Major tectonic features are redrawn from Awasthi (2017), Imsong et al. (2016) and Liu et al. (2016b). Regions demarcating the Woyla Arc, West Sumatra, are from Advokaat et al. (2018) and West Burma block from van Hinsbergen et al. (2011). Red box demarcates the Andaman Islands and Rutland Island (detailed in Fig. 1b); previous geochronological results are also shown (see text for details). Relief data are from ETOPO1 Global Relief Model (http://www.ngdc.noaa.gov/mgg/global/); (b) Geological map of Andaman Islands (modified after Ghosh et al., 2017) over processed-hillshade map (generated using SRTM digital elevation data with a resolution of 1 arc-second from USGS Earth Explorer https://earthexplorer.usgs.gov/; modified after Bandyopadhyay et al., 2020). North-South extending Jarwa Thrust is also shown. STDS: South Tibetan Detachment System, MCT: Main Central Thrust, MBT: Main Boundary Thrust, MFT: Main Frontal Thrust; LA: Little Andaman; CN: Car Nicobar; Nic. I: Nicobar Islands; GN: Great Nicobar; EMF: Eastern Margin Fault; DF: Diligent Fault; WAF: West Andaman Fault; BI: Barren Island; NI: Narcondam Island; AR: Alcock Rise; SR: Sewell Rise; WOB: Western Ophiolite Belt; MOB: Myitkyina Ophiolite Belt. Star marks indicate important field locations of Middle and South Andaman and Rutland Island that are discussed in this study (sample locations are marked by green stars, see text for details); (c) Google Earth satellite image showing the salient locations along the Panchawati coast (Middle Andaman).

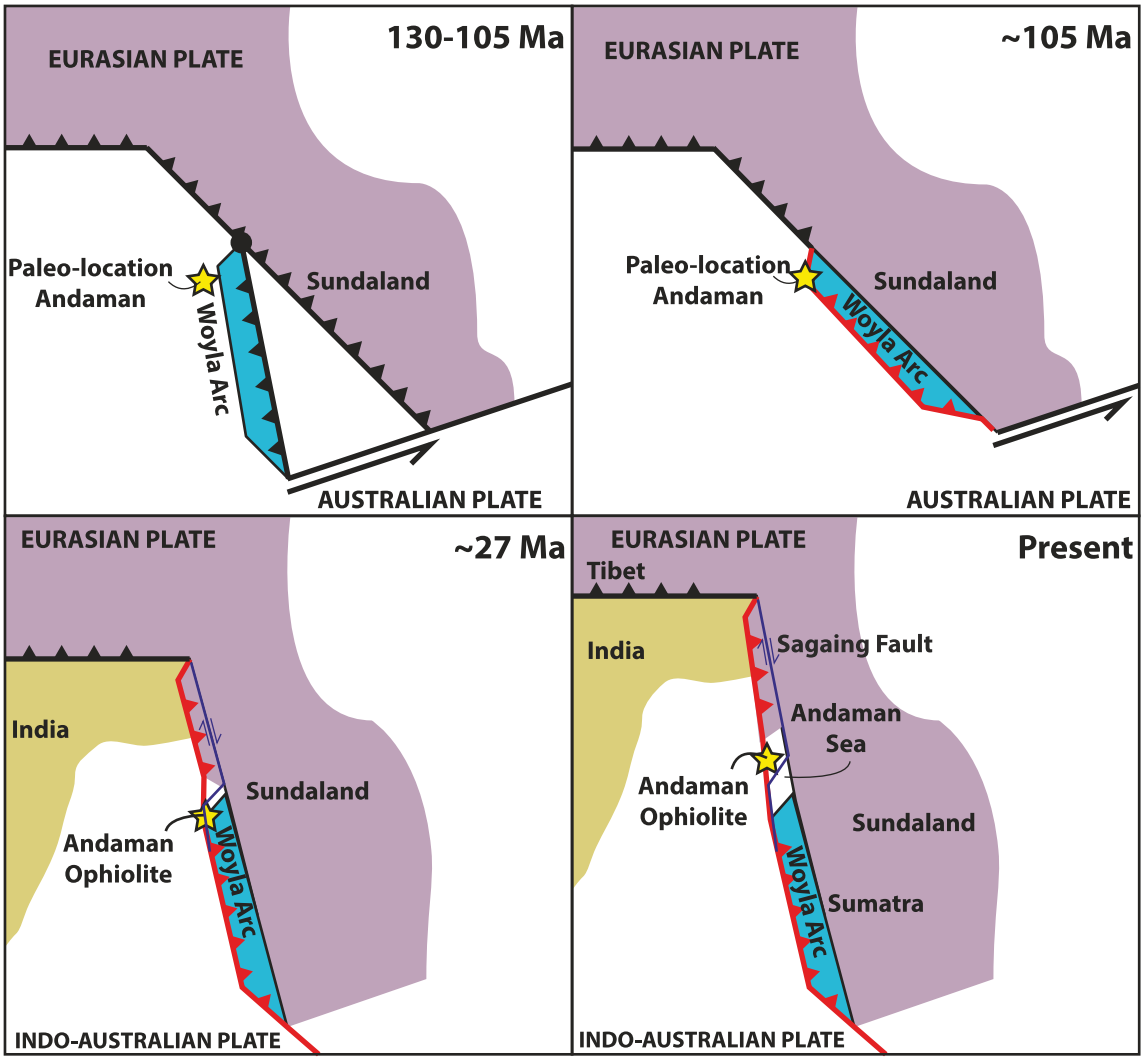

Fig. 2. Schematic plate kinematic reconstruction of the east Indian Ocean from the Cretaceous to the present, with the predicted location of Andaman, modified from Advokaat et al. (2018).

1.3 Ma (Sarma et al., 2010) and 95 ± 2 Ma (Pedersen et al., 2010) show that by this time, the Andaman Ophiolites were located above and close to a subduction zone. Thus, explaining the formation of the Andaman Islands as a regular SSZ ophiolite may be tempting (Pedersen et al., 2010).

However, the existing geochemical and geochronological constraints of the Andaman Ophiolite appear to be more diverse than straightforwardly explained in such a setting (Bandyopadhyay et al., 2020; Ghosh et al., 2017, and references therein). Specifically, the presence of less depleted lherzolitic mantle, the geochemical characteristics of which are more common for a back-arc basin instead of a SSZ ophiolite forearc spreading centre (Ghosh et al., 2018). In addition, the ophiolite is associated with explosive volcanic agglomerates that are indicative of mature arc volcanism, all within the same ophiolite suite, within a few kilometres from each other (Fig. 1b,c). Moreover, $^{40}Ar/^{39}Ar$ cooling ages of the Andaman metamorphic sole were recently shown to give ~105 Ma ages (Plunder et al., 2020), i.e. 10–12 Myr older than the subduction-influenced plagiogranites. This is surprising because globally there is a coincidence between sole cooling and supra-subduction zone ophiolite spreading (Dewey and Casey, 2013; van Hinsbergen et al., 2015). So, does the Andaman ophiolite challenge general ophiolite concepts? Or else, does it juxtapose magmatic and metamorphic rocks formed in different settings at different times?

A recent kinematic reconstruction of the eastern Indian Ocean provides predictions on the sequence of tectonic settings that the Andaman Ophiolites may have experienced through time (Fig. 2). In this paper, we aim to evaluate this reconstruction of the geochemical and geochronological record of the Andaman Sea. The reconstruction first restores the N-S opening of the Cenozoic Andaman Sea Basin to the east of the Andaman Islands, which brings the ophiolites to the west of Sumatra (van Hinsbergen et al., 2011). On western Sumatra lies the intra-oceanic Woyla Arc that collided with the Sundaland continent of SE Asia around 100 Myr ago (Advokaat et al., 2018; Barber et al., 2005). Prior to collision, there was westward subduction below the Woyla Arc (Barber et al., 2005), implying that the subduction zone that produced the Andaman metamorphic soles and arc magmatic rocks formed in the former back-arc region behind the Woyla Arc (Advokaat et al., 2018).

In this paper, we critically re-evaluate the field relationships and geochemical and geochronological constraints on the Andaman Ophiolite and its metamorphic sole, and present new geochemical results for the metamorphic sole and igneous rocks. We also present new zircon U–Pb geochronological results from gabbros and plagiogranites from three new locations of Middle Andaman, South Andaman, and Rutland Island. Finally, we then evaluate whether the geochemical and geochronological characteristics of the Andaman

Ophiolites may be readily explained in the context of the regional plate kinematic evolution.

2. Geological framework

The Andaman and Nicobar archipelago, a chain of islands in the NE Indian Ocean, stretches for over 700 km, with a maximum width of c. 60 km, in the forearc of the Sunda subduction zone (Fig. 1a). This archipelago occurs as the exposed part of a long ridge which extends from the Arakan–Yoma ranges of western Myanmar in the north to Sumatra in the south, and is flanked by the Andaman Sea to the east and the Bay of Bengal to the west (Fig. 1a; Bandopadhyay, 2017). Ophiolitic rocks in the Andaman and Nicobar islands were first reported by Karunakaran et al. (1964) and described as dismembered bodies (Hutchison, 1975). Being located between the Himalayan collision zone and the Indonesian arc system, this ophiolite has the potential to offer insights into the Tethyan tectonics and India-Asia collision as a whole, though natural isolation along with geographical inaccessibility left these islands unexplored for long. In the 1980-1990's a few geological investigations were carried out on the Andaman ophiolite (Acharyya et al., 1990; Jafri et al., 1990, 1995; Ray, 1985; Ray et al., 1988). In the last decade, especially after the great 2004 Sumatra-Andaman earthquake, and after recent volcanic eruptions on Barren Island in the active arc east of the Andaman islands, a significant amount of research has appeared in the international literature (Lay et al., 2005; Meltzner et al., 2006; Morishita and Ghosh, 2010; Pal et al., 2007, 2010; Sheth, 2014). Following that, many workers have focused on the ophiolites and other lithomembers of the islands to understand their evolution and bearing on regional plate tectonics (Bandopadhyay, 2012; Bandyopadhyay et al., 2020; Ghosh et al., 2009, 2017; Pal, 2011; Pal et al., 2003; Pedersen et al., 2010; Sarma et al., 2010).

The Sunda trench in the Andaman region is accommodating highly oblique convergence between the Indo-Australian and Eurasian plates (Curray, 1989). To the north, the Sunda trench connects to the collisional margin between India and the west-Burma block (Myanmar), and the Main Frontal Thrust of the Himalaya (Fig. 1). The oceanic subduction to the south has resulted in an active volcanic arc extending from Sumatra to the central Myanmar Basin in north Myanmar, including two volcanic islands in the Andaman Sea - Barren and Narcondam (Acharyya, 2007).

The Andaman Sea basin is a pull-apart basin that links two main strike-slip corridors: the Sagaing Fault between the West Burma Block of Myanmar to the northeast, and the West Andaman and Old West Andaman Faults and the Sumatran Fault System to the southwest (Fig. 1a). This fault system separates the West Burma-Andaman forearc sliver from Sundaland and transferred it northward. Since the Late Pliocene, extension in the Andaman Sea was accommodated by oceanic spreading (Curray, 2005; Kamesh Raju et al., 2004). Prior to that time extension was accommodated by crustal stretching, with cooling ages of exhumed dredge samples from the Alcock and Sewell Rises adjacent to the Andaman oceanic basin suggesting Early Miocene extension and exhumation (Curray, 2005; Frerichs, 1967; Rodolfo, 1969a, 1969b). Oligocene extension was documented in the Mergui-North Sumatran basin (Andreason et al., 1997; Kamili et al., 1976; Polachan and Racey, 1994), which suggests that the formation of the Burma-Andaman sliver plate started sometime in the Oligocene, consistent with recent findings of Sagaing Fault activity at 27.5 Ma (Morley and Arboit, 2019). Restoring all this extension brings the southern margin of the West Burma Block adjacent to north Sumatra, and the northern margin of the West Burma Block to the south of the major Eo-Oligocene Mae Ping and Three Pagodas faults that cut NW-SE through mainland Indochina, but not through the West Burma Block (van Hinsbergen et al., 2011).

This restoration also brings the Andaman ophiolites to the west of North Sumatra (Advokaat et al., 2018; van Hinsbergen et al., 2011), immediate west of the Woyla Arc. This arc complex consists of basaltic to andesitic volcanic rocks that include xenoliths of radiolarian chert, dykes, and volcaniclastic sandstones lacking quartz, and shales, with no indications that the arc was built on a continental basement (Barber, 2000; Wajzer et al., 1991). It is a Cretaceous (~130–105 Ma) intra-oceanic arc, thought to have formed above a W-dipping, intra-oceanic subduction zone that terminated upon collision with continental Sundaland (Barber et al., 2005). Following collision, the subduction polarity switched and became northeastward, like today, with the accreted Woyla Arc in an upper plate position (Advokaat et al., 2018; Barber, 2000; Barber et al., 2005; Wajzer et al., 1991). Advokaat et al. (2018) postulated that the initiation of subduction recorded in the Andaman Ophiolites is causally related to the arrest of subduction upon collision of the adjacent Woyla Arc.

Recently, Plunder et al. (2020) estimated 105–106 Ma Ar/Ar cooling age from amphibolites of dismembered metamorphic soles of the Andaman ophiolite, which is at least 10 Myr older than the previous magmatic ages from the plagiogranite. Such metamorphic soles are thought to represent the uppermost slices of downgoing oceanic lithosphere that became metamorphosed and accreted beneath the upper plate lithospheric mantle during ophiolite spreading (e.g. Agard et al., 2016; Guilmette et al., 2008, 2009, 2012; Soret et al., 2017; van Hinsbergen et al., 2015). Whilst metamorphic soles may form well before suprasubduction zone spreading (Guilmette et al., 2018; Pourteau et al., 2019), their cooling ages are systematically synchronous with the age of SSZ spreading (van Hinsbergen et al., 2015). Therefore, Plunder et al. (2020) argued that the 93–95 Ma ages of the plagiogranites do not reflect SSZ spreading of the Andaman ophiolite, but rather the development of a mature arc in and on already existing SSZ crust, which then likely is 105 Ma old. Such an age was reported from a plagioclase xenocryst hosted in a recent Barren Island lava flow (Ray et al., 2015).

Towards the north, in the Indo-Burman Ranges, there are ophiolites with Early Cretaceous (116–133 Ma) crust (Aitchison et al., 2019; Liu et al., 2016a; Singh et al., 2017; Zhang et al., 2018). Because these are presently a part of the same forearc system as the Andaman-Nicobar Accretionary Ridge, they are widely assumed to have formed at the same subduction zone as the Andaman-Nicobar ophiolites (e.g. Liu et al., 2016a). Advokaat et al. (2018) conceptually explained the southward younging trend in the ophiolites as the result of a southward migration of a triple junction during the polarity reversal documented at Sumatra. However, recent paleomagnetic data from Westerweel et al. (2019) suggested that the Indo-Burman Ranges were located at the same latitude as Sumatra in the Cretaceous to Eocene. This implies that these blocks, and the ophiolites in their forearcs, were parts of different plates, and hence at different plate boundaries. In this paper we focus, therefore, on the Andaman Ophiolite and leave the relation with ophiolites in the Indo-Burman Ranges for future study.

3. Ophiolitic lithologies - field relationships and geochemical fingerprinting

Most of the Andaman islands are occupied by dense tropical forest and exposure is mostly restricted to coastal, river, and rare road outcrops. Exposures reveal ophiolitic rocks and underlying metamorphic sole and mélange, an overlying Paleogene–Neogene turbidite sequence of clastic sedimentary rocks (Fig. 1b; Bandopadhyay and Carter, 2017). Below we will briefly summarize the field relationship of the different ophiolitic litho-units along with the published geochemical and geochronological results, with special emphasis on the location-specific field disposition, which we believe holds the clue to resolve the existing gap areas regarding the genesis of this ophiolite.

The Andaman ophiolite suite, including the underlying sole and mélange rocks, is found in the hanging wall of the prominent, N-S striking Jarawa (or Jarwa) Thrust that runs over the central-western part of the Andaman Islands (Fig. 1b). This thrust juxtaposes the ophiolite suite and overlying Paleogene sedimentary sequence westwards upon an accretionary prism of deep-marine, presumably post-Eocene turbidite

sequences (Fig. 1b; Bandopadhyay and Carter, 2017). The Andaman ophiolite suite consists of tectonized, restitic mantle sequences (>700 m thick in North Andaman Island) that host chromitite pods, a plutonic crustal section mainly exposed as cumulate rocks (up to 150 m thick), and volcanic rocks (up to 400 m thick in South Andaman); notably with exposures mostly restricted to the east coast of North, Middle, South Andaman and Rutland Islands (Ghosh et al., 2009, 2013, 2017; Pal, 2011). Identifying the components of an idealized 'Penrose' (Anonymous, 1972) architecture of the oceanic lithosphere has been attempted for the Andaman ophiolite (Pal, 2011; Saha et al., 2010). However, it is important to note that while some elements of the Penrose sequence are present (peridotites, gabbros, pillow lavas, cherts, but sheeted dykes are absent), there is nowhere a coherent sequence exposed and contacts between ophiolitic rock units are poorly exposed. This may be a result of tectonic dismemberment, because the sequence has always been incomplete, and/or because there is a multiphase magmatic history preserved that is not typical for a Penrose sequence. In any case, the Andaman ophiolite suite contains different ophiolitic lithomembers, cropped out in various islands, that are put together in an ophiolite stratigraphy (Bandyopadhyay et al., 2020; Ghosh et al., 2017).

3.1. Metamorphic sole

Metamorphic rocks, comprising sheared meta-volcanics and meta-sediments, have been found confined to either the base of the ophiolite, immediately below the mantle peridotite (in North Andaman) or as subangular blocks within the mélange (in Middle Andaman) (Pal et al., 2003). Pal and Bhattacharya (2010) interpreted these metamorphic rocks as the sub-ophiolitic greenschist facies rocks representing the sole of ophiolite slices (e.g. Wakabayashi and Dilek, 2003). Geochemically, protoliths of the metabasites are inferred to be subduction influenced (Pal and Bhattacharya, 2010). Towards south, along the Panchawati coast, Middle Andaman (*Location 1–12°35′34"N; 92°57′26″ E;* Fig. 1b, c), we document different lithotypes occurring as blocks of up to 10 m or more in a serpentinite matrix (see also Plunder et al., 2020). The rock types include metabasite (amphibolite), peridotite, mafic rocks, and metachert. These were emplaced over Paleogene clastic sedimentary rocks along a post-Paleogene thrust. The peridotite boulders along the coast are inferred to be the same as the to lherzolitic mantle peridotite (Ghosh et al., 2018) exposed in a nearby quarry section (Ghosh et al., 2013). Plunder et al. (2020) estimated peak metamorphic conditions for the sole amphibolites of ~0.9 GPa and ~ 675 °C, followed by cooling below closure temperatures for argon in hornblende (~500 °C) constrained by $^{40}Ar/^{39}Ar$ ages of 106.4 ± 2.1 Ma and 105.3 ± 1.6 Ma.

3.2. Mantle section

Previous work on the mantle section of the Andaman ophiolites has yielded disparate estimates of its chemical history (Ghosh et al., 2009, 2013, 2018; Pal, 2011). Peridotites are variably serpentinised (40–80 vol%) and display strong post-serpentinization deformation across the Andaman Islands. Locally, a crude primary foliation is discerned in the least serpentinized samples. Petrography and mineral chemistry of the mantle sequence of the Andaman ophiolite portray a pronounced variation between Rutland Island in the south and Middle and North Andaman towards the north (Ghosh et al., 2013). In Rutland Island and South Andaman, mantle rocks are mainly harzburgite-dominated where chrome spinel and clinopyroxene compositions suggest them to be residue of 14–18% melting of a fertile mantle (e.g. DMM; Workman and Hart, 2005) in a SSZ environment (Ghosh et al., 2009, 2018). On the other hand, the mantle peridotites in Middle and North Andaman Island are fertile lherzolite that occasionally grades to clinopyroxene-bearing harzburgite, corresponding to <10% mantle melting with minor flux infiltration (Morishita et al., 2018a), with a geochemistry suggesting formation in a back-arc setting (Ghosh et al., 2018). Massive chromitite pods of 8–20 cm size (maximum up to 50 cm) within harzburgite have been reported from Rutland Island (Ghosh et al., 2009) whereas the same pods in lherzolitic mantle rocks have been reported from North-Andaman (Ghosh et al., 2013; Ghosh and Bhatta, 2014).

3.3. Transition between mantle and crustal rocks

Ghosh et al. (2014) interpreted a nearly 6 m thick zone along a road-cut section at Kodiaghat, South Andaman, exposing olivine-rich troctolite with evidence of being overlain by clinopyroxenites, wehrlites and gabbroic rocks, as a MOHO transitional zone *(Location 2–11°31′ 21"N; 92°43′08″E)* (Fig. 1b, 3a,b). Ghosh et al. (2014) described field relationships and clinopyroxene compositions that suggested a genetic link between olivine-rich troctolite, the layered gabbros, and the clinopyroxenite-wehrlite association. They also inferred from the chrome spinel composition that the olivine-rich troctolite was eariler a dunite formed by interaction between melt and a mantle similar to the depleted harzburgite of Rutland Island.

3.4. Crustal section

The lithotypes belonging to the crustal section of the Andaman ophiolite are less abundant than mantle rocks and best exposed in South Andaman along a road section on the way to Chidiyatapu (Fig. 1b), as well as in Rutland Island. The crustal section comprises continuous layered gabbroic rocks at its base, followed up-section by various plutonic rocks collectively named as high-level intrusives, and volcanics at the top. Layered gabbroic rocks, immediately above the cumulate sequence of the MOHO transition zone, are best exposed in the Kodiaghat section, South Andaman *(Location 2–11°31′21"N; 92°43′08″ E)* (Figs. 1b, 3a,b) (Ghosh et al., 2014; Pal, 2011). A wide variation in modal mineralogy has been documented within interlayered olivine gabbros (Ghosh et al., 2014, 2017). A coastal exposure in Bedonabad *(Location 3–11°34′01"N; 92°44′10″E)* (Fig. 1b) displays a variety of plutonic and volcanic-hypabyssal rocks. At this location we have found homogeneous gabbro (noncumulate gabbro) and a plagiogranite-diorite suite, together termed as 'high-level intrusives' (Pal et al., 2003). The plagiogranite-diorite suite and volcanic-hypabyssal rocks are often intermingled (Fig. 3c). Locally the plagiogranite appears intrusive within gabbro as irregular bodies (Jafri et al., 1995). Zircon from this plagiogranite yielded an age of 93.6 ± 1.3 Ma (Sarma et al., 2010). Plagiogranite and the non-pillowed volcanic rocks, wherever present, appear brecciated and we describe them as magmatic breccia. Near-vertical thin dykes of altered dolerite are common. We also documented basaltic enclaves within the plagiogranite-diorite suite. Plagiogranites of this location display a volcanic arc geochemical signature (Jafri et al., 1995). In Middle Andaman, an in-situ exposure (*Lat: N12°34′45″; Long: E92°57′41″*) (Fig. 1b,c) of leucocratic rocks belonging to the diorite – granodiorite series is in close association with agglomerates (Fig. 3d), suggesting a genetic linkage between the two. On Rutland Island, plagiogranite *(Location 4–11°24′10"N; 92°39′34″E)* (Fig. 1b) is locally exposed along the south-eastern coastal tract of the island, as small dyke-like bodies showing mutually intrusive relationships with gabbro (Fig. 3e). Sheeted dyke complex has not been observed in the Andaman ophiolites (Ghosh et al., 2017).

Amongst the crustal rocks, volcanic units dominate. Two distinct groups of volcanic rocks – dubbed 'pillow lavas' and 'East Coast volcanics' were reported from the Andaman ophiolite based on their field characteristics (mainly in South Andaman) and geochemical affinity (Ghosh et al., 2017, and references therein). The 'East Coast volcanics', with oceanic island arc affinity, occur as separate thrust slices over the 'Pillow lavas' (Ray, 1985; Ray et al., 1988). An alternative classification proposed by Vohra et al. (1989), coined 'upper lava' for pillow basalts

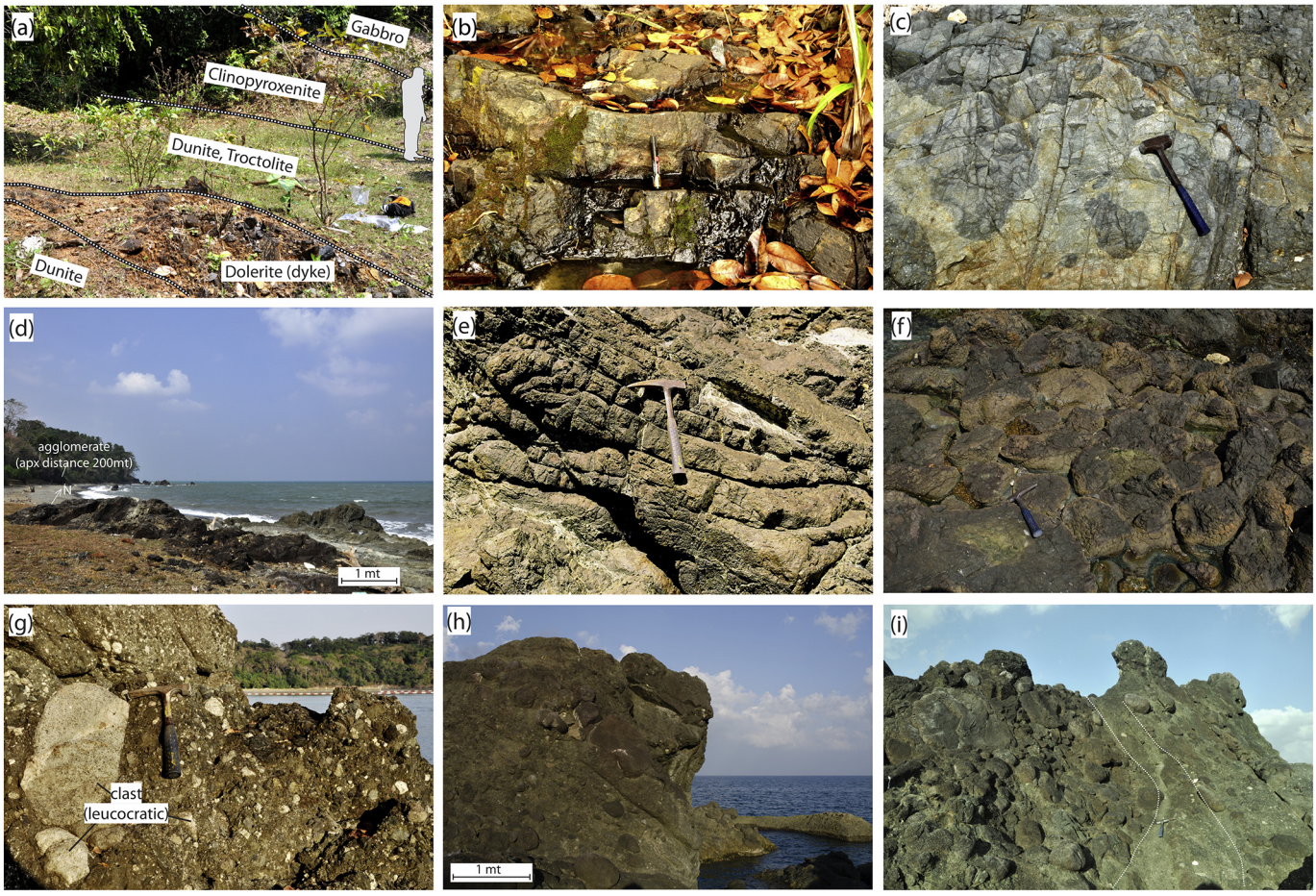

Fig. 3. Field disposition of different magmatic rocks in the Andaman Islands - (a) Rock types exposed in the MOHO Transition zone (MTZ) in Kadiaghat, South Andaman (Location 2, see Ghosh et al., 2014 for details); (b) In-situ exposure of layered gabbro in South Andaman, in close proximity of the MTZ location (location 2); (c) Plagiogranite exposure on the Bedonabad coast, South Andaman (location 3), Note the intermingling of mafic rocks with the plagiogranites; (d) In-situ exposure of leucocratic rocks (belonging to the diorite – granodiorite series) in close association with agglomerates on the Panchawati coast, Middle Andaman (location 1); (e) Plagiogranite exposure in Rutland Island (location 4); (f) Pillow lava outcrop at Corbyn's Cove beach, South Andaman (location 5); (g) Coastal exposure (near Mundapahar beach) of agglomerates in Chidiya Tapu, South Andaman (location 6). Note the predominant occurrence of felsic blocks of varied size; (h, i) Coastal exposure of agglomerates on the Panchawati coast, Middle Andaman (location 1).

and 'lower lava' for the East Coast volcanic rocks, interpreted to tectonically overlie the former (see table 7.2 of Ghosh et al., 2017).

In South Andaman Island, a coastal exposure *(Location 5 – Corbyn's Cove, South Andaman; 11°38′28″N; 92°44′50″E)* preserves tholeiitic pillow basalts (Ray et al., 1988) (Figs. 1b,3f). Hyaloclastites and (brecciated) pillow lavas with MORB geochemical affinity have been reported from this location (Jafri et al., 2010). Non-pillowed East Coast volcanic rocks are found in the coastal exposure in Bedonabad, South Andaman, *(Location 3–11°34′01″N; 92°44′10″E)*. Ray et al. (1988) also concluded that the East Coast volcanics (basaltic andesite, acid volcanics) are genetically connected with the tholeiitic pillow basalts and formed on a marginal basin floor. Alternatively, a plume origin (Jafri et al., 1990) and a mid-ocean ridge setting (Srivastava et al., 2004) have been also proposed for the South Andaman volcanic rocks. With progressive development of the ophiolite concept, the South Andaman volcanic rocks, with a spectrum of geochemical variation - from MORB to boninites to evolved arc volcanics, have been linked with different stages of subduction by Pal (2011). This was later supported by Bhattacharya et al. (2013) based on volcanic rocks from Rutland Island. Close to the MOHO Transition Zone exposure of the Kodiaghat section, South Andaman *(Location 2–11°31′21″N; 92°43′08″E,* Fig. 1b*)* Ghosh et al. (2014) reported East Coast volcanic samples with a similar geochemical signature to that of calculated melt compositions in equilibrium with clinopyroxene from olivine-rich troctolites and gabbroic rocks.

Near Chidiya Tapu (farther south from location 2, near to Mundapahar beach, *Location 6–11°29′33″N; 92°42′18″E,* Fig. 1b) we documented a ca. 100 m long coastal exposure that preserves an extensive agglomerate volcanic facies with a bimodal composition of clasts, consisting of mafic-intermediate volcanic rocks (andesite, dacite) and dominantly plagiogranite (Fig. 3g). The size, angularity and composition of the clasts vary from bomb to block tuff. Pedersen et al. (2010) reported a 95 ± 2 Ma age from a plagiogranite in South Andaman. Based on the location marked on their map and description that "the dated trondhjemite (plagiogranite) was sampled at a coastal exposure at Chidiya Tapu at the southern tip of South Andaman Island, where it occurs together with gabbros and cross-cutting dykes", we have tried to access the location to document the relationship between volcanics and intrusives. Trondhjemite (plagiogranite) dykes mentioned by Pedersen et al. (2010) are not exposed at Chidiya Tapu and we presume that their 95 ± 2 Ma age dates the plagiogranite blocks contained in the agglomerate and formed during an explosive volcanic eruption. Geochemical investigation further inferred that they formed in a supra-subduction zone environment (Bhattacharya et al., 2020).

Volcanic agglomerates are abundant along the Panchawati coast, Middle Andaman *(Location 1–12°35′34″N; 92°57′26″E*; Fig. 1b,c),

where they form coherent blocks of tens of m across. The interlayered pyroclastic rocks are dominantly composed of andesitic (Pal and Bhattacharya, 2016) blocks of different sizes (m to cm scale), sorted in layers set in a volcanic matrix of andesitic composition (Fig. 3h,i). It is not clear whether these are located within the mélange, or whether they belong on top of the ophiolite and were overthrust by the mélange along post-Paleogene thrusts that cut the ophiolite and overlying Paleogene clastic sequence. The latter option appears more likely as serpentinite-matrix mélanges including metamorphic sole blocks are located adjacent to the agglomerates, which do not appear internally deformed, or metamorphosed, and the agglomerates contain plagiogranites (in South Andaman) that are also found intruding the ophiolite.

Various hemipelagic sedimentary rocks are documented along a ~ 3 km stretch of the Panchawati coast (*Location 1–12°35′34″N; 92°57′26″E;* Fig. 1b). They constitute a volumetrically minor component in the Andaman ophiolite, occur either alternating with basalt or in short successions (~ 2.5 m thick) immediately overlying the extrusives. They are characterized by thin layers of red and light green mudstone, greenish and red chert, and limestone. Jafri et al. (1993) reported radiolarian cherts from South Andaman in association with pillow basalts (near Bedonabad), conglomerate and grit (near Bamboo flat). Several biostratigraphic age constraints have been proposed from hemipelagic sediments - Early Cretaceous based on radiolarian assemblage (Jafri, 1986); Early Eocene to Paleocene from radiolaria in red cherts and planktonic foraminifera in limestones (Roy et al., 1988); Eocene (Middle) and Cretaceous (Campanian) from radiolarian faunas (Ling et al., 1995, 1996; Ling and Srinivasan, 1993); Late Cretaceous to Paleocene (Pal et al., 2003). However, the field disposition of the cherts, from which this large spectrum of ages was determined, is poorly described in the literature, thus their stratigraphic position and formation with respect to the ophiolite is difficult to assign. Jafri et al. (2006) documented the presence of ash layers in radiolarian cherts in South Andaman and correlated them with a possible explosive volcanic event related to the East Coast volcanics during the Late Cretaceous.

4. Methodology

4.1. Geochemistry – Sampling rationale and analytical techniques

Whilst extensive geochemical analyses have previously been performed on the ultramafic and mafic rocks of the Andaman Ophiolite suite (Ghosh et al., 2017, and references therein) no detailed and comprehensive geochemical analyses were previously reported from the pyroclastic agglomerates of South Andaman and Middle Andaman, nor for the amphibolites of the metamorphic sole. To aid the tectonic interpretation, we collected representative samples of agglomerates from the Chidiya Tapu coastal exposure (location 6) and Panchawati coast (location 1), as well as amphibolites from Middle Andaman. These amphibolites are studied in detail for metamorphic and thermochronological analysis by Plunder et al. (2020). Petrographic data of the selected samples are shown in Fig. 4 and Table 1. Based on this, fourteen samples were chosen for whole rock geochemistry (major and trace elements) (Table 2; Figs. 5,6). All samples were analysed at Actlabs (Canada) using the Lithoresearch package methodology.[1] Analyses for blanks, replicates and standards are provided in supplementary material.

4.2. U/Pb geochronology

4.2.1. Sampling rationale

Previous geochronological studies on South Andaman plagiogranites gave 93–95 Ma ages for supra-subduction magmatism (Pedersen et al., 2010; Sarma et al., 2010). Because these plagiogranites are found in association basaltic andesitic agglomerates with island arc geochemical affinity (see above), which is consistent with the geochemistry of the plagiogranites (Jafri et al., 1995; Bedonabad coast, location 3), Bandyopadhyay et al. (2020) suggested that the subduction initiation below the Andaman ophiolites may be older than the 95 Ma plagiogranite ages, as confirmed by the $^{40}Ar/^{39}Ar$ plateau ages of ~105–106 Ma of the metamorphic sole (Plunder et al., 2020), as well as the plagioclase xenocrysts hosted in a Barren Island lava flow (Ray et al., 2015). We have collected samples suitable for U–Pb zircon analysis from the previously undated outcrops in Middle Andaman and Rutland Island to test the robustness of the previous ages.

We also selected a layered gabbro from the Kadiaghat section, South Andaman that is geochemically linked to the East Coast volcanics (Ghosh et al., 2014). Dating the crystallization of this gabbro would provide constraints on the timing of the magmatic event from which resulted the East Coast volcanics. From the collected samples, three (marked in Fig. 1b) - **148A** *[Lat: N11°24′10″; Long: E92°39′34″; Rutland Island (location 4)]*; **SA-GAB1** *[Lat: N11°31′57″; Long: E92°43′25″; South Andaman (location 2)]* and **L-18** *[Lat: N12°34′45″; Long: E92°57′41″; Middle Andaman (location 1)]* proved to be most suitable for further geochronologic investigation. Petrographic description of the samples is in Table 1.

4.2.2. Analytical techniques

Zircon grains were extracted by crushing, milling and separation using a Wilfley table, and concentrated using a combination of magnetic separators and heavy liquids (methylene iodide). Individual grains were selected under an optical microscope and subjected to chemical abrasion (Mattinson, 2005). This was followed by spiking with a ^{202}Pb-^{205}Pb-^{235}U tracer, dissolution, and mass spectrometry, after the procedure detailed in Krogh (1973) with modifications described in Corfu (2004). For small amount of Pb measurements were performed with an ion counting secondary electron multiplier. The obtained data were corrected with fractionation factors for Pb determined from the measured $^{202}Pb/^{205}Pb$ of the added spike and for U by 0.12%/amu. Blank corrections were 0.1 pg for U and ≤ 2 pg Pb. Additional common Pb in one fraction was corrected using a composition calculated with the model of Stacey and Kramers (1975). The data were also adjusted for a deficit of ^{206}Pb due to initial deficiency of ^{230}Th (Schärer, 1984) and the tracer was calibrated with reference to the ET100. Plotting and regressions were done with the Isoplot software package (Ludwig, 2009). The decay constants are after Jaffey et al. (1971). Detailed geochronological results are given in the section 5.2, Table 3, and Fig. 7.

5. Results

5.1. Geochemistry

We first note that most of the samples contain more than 1 wt% volatile (LOI), with a few agglomerates containing more than 5 to 10 wt% LOI. Such volatile contents are potentially indicative of elemental mobility during hydrothermalism or metamorphism (for example, Ca, Na and K are susceptible to mobility during greenschist and amphibolite facies and Si, Fe and Mg during high fluid-rock ratios in the hydrothermal systems). Accordingly, all ensuing interpretation and discussion will rest on ratios between elements deemed immobile (e.g. Ti, Zr, Y, Nb etc.,) during hydrothermal alteration/metamorphism (e.g. Cann, 1970; Pearce, 1975; Pearce, 2014; Pearce and Cann, 1971; Shervais, 1982).

5.1.1. Major and minor elements

We first characterize our geochemical dataset with major element based binary, Harker-type diagrams (Fig. 5). To this end, we recalculated the bulk rock analyses on an anhydrous basis to avoid the closure effect of high LOIs, and adjusted FeO and Fe_2O_3 as per Fe^{2+}/

[1] available online https://actlabs.com/geochemistry/lithogeochemistry-and-whole-rock-analysis/lithogeochemistry/

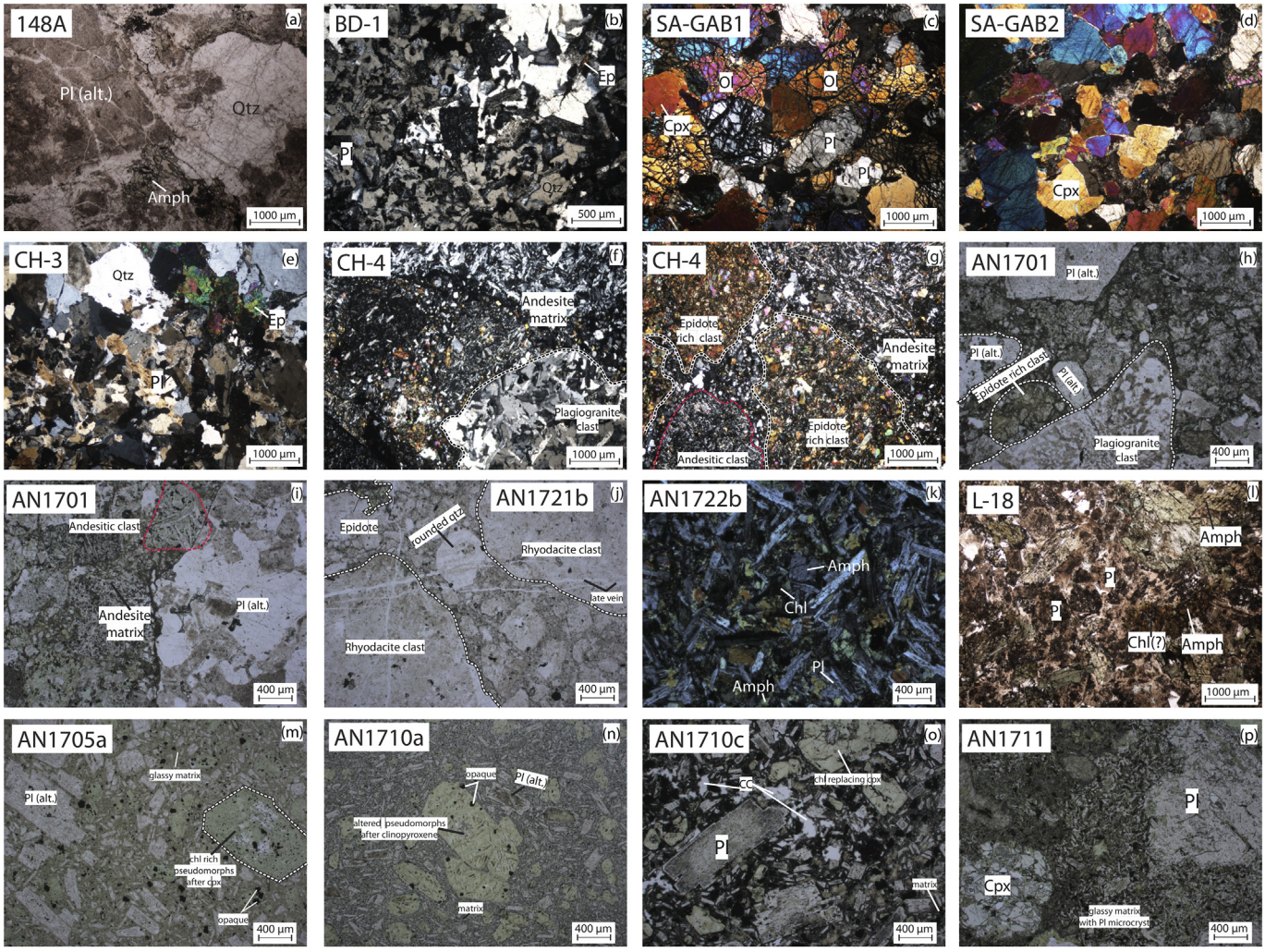

Fig. 4. Optical photomicrographs showing characteristic petrographic features – (a) plagiogranite (148A), note plagioclase grains are often altered; (b) plagiogranite (BD-1) showing interstitial vermicular and micrographic intergrowths of quartz and plagioclase; (c) layered gabbro (SA-GAB1) composed of olivine, plagioclase, clinopyroxene and showing cumulate texture; (d) cumulate clinopyroxenite (SA-GAB2) with interstitial plagioclase; (e) plagiogranite clast from the agglomerates (CH-3) with hypidiomorphic granular texture, note the occurrence of epidote; (f-k) agglomerates from South Andaman that contains varieties of clasts (e.g. plagiogranite, andesite, epidote-rich clasts etc.) in fine grained volcanic matrix; (l) leucocratic rock belonging to the diorite – granodiorite series (L-18) showing hypidiomorphic granular texture, composed of plagioclase and amphibole (locally replaced by chlorite); (m-p) volcanic rocks (agglomerates) from Middle Andaman, dominantly showing porphyritic texture. Besides plagioclase there are phenocrysts of another phase, possibly clinopyroxene, replaced by chlorite and carbonate (See Table 1 for details).

Fe_{tot} = 0.85 (e.g. Schilling et al., 1983). Amongst the five analysed metamorphic sole samples from Middle Andaman, three amphibolite samples have a basic-intermediate transitional composition with SiO_2 = 50–53 wt% (Fig. 5). Two samples have outlying compositions; AN1704a with ~58.5 wt% SiO_2 belongs to the intermediate group (Fig. 5), whereas AN1703 is acidic with SiO_2 ~ 90 wt%. Its quartz-rich nature (up to 70%) with less than 10% amphibole suggests a non-volcanic protolith (probably meta-chert). Its chemistry will hence not be discussed further. The three basic-intermediate samples share similar compositions consistent with a primitive basalt protolith, with 1.3–1.5 wt% TiO_2 (Fig. 5a), ~13–14 wt% Al_2O_3 (Fig. 5b) and 9–10% CaO (Fig. 5c). Their Mg#, Cr and Ni contents are also typical of primitive basalts with values in the range of 0.61–0.63 (Fig. 5d), 170–280 ppm (Fig. 5e) and 80–170 ppm (Fig. 5f), respectively. By contrast, sample AN1704a has a much lower TiO_2 (0.5 wt%) and CaO (7 wt%) contents, similar Al_2O_3 (13.4 wt%) and significantly higher Mg# (0.72), Cr (410 ppm) and Ni (280 ppm) contents, hinting to a different protolith. Considering that the primary structures and textures of rocks from the metamorphic sole have been obliterated during tectonometamorphism, we tested the chemistry of the studied samples in a Mg# vs. SiO_2/Al_2O_3 (Kempton and Harmon, 1992) diagram (Fig. 5g) to identify samples that could have had cumulates as a protolith (excluding siliceous sample AN1703). The three samples with clustered compositions plot within the field of primitive basalts, confirming that their protoliths are representative of magmatic liquids and not cumulates. The outlying composition of sample AN1704a appears to result from the accumulation of pyroxene, consistent with its higher Cr and Ni contents. The sample still plots close to the field of primitive basalts, possibly representing pyroxene-phyric lava.

Intermediate agglomerate samples from Middle and South Andaman have relatively clustered compositions except for outlier sample AN1721b, petrographically identified as brecciated rhyodacite (Table 1, Fig. 4j). This classification is consistent with its very high SiO_2 (~79 wt%), lower TiO_2 (0.27 wt%), Al_2O_3 (11 wt%) and Mg# (0.27), with undetectable Ni and Cr (Fig. 5a-f). All other agglomerate samples have intermediate compositions with SiO_2 ~ 53–58 wt% (Fig. 5a). TiO_2 is also fairly consistent across samples with contents ranging between 0.6 and 1.0 wt% (Fig. 5b). The Al_2O_3 and CaO contents are strongly variable, ranging between 15 and 20 wt% and 0.5–9 wt% respectively (Fig. 5c,d), and inversely correlated. The very low CaO

Table 1
Geographic location and petrographic summary of the studied samples of Andaman ophiolites.

Sample	Coordinate		Island	Rock type	Petrographic feature	Geochemistry	Geochronogy
148A	11°24′ 10″N	92°39′ 34″E	Rutland Island	Plagiogranite	Dominantly composed of plagioclase (often saussuritized), amphibole and quartz. Amphibole is replaced by chlorite and quartz is often recrystallized. Intergranular spaces between larger plagioclases are composed of granular aggregate of smaller plagioclase and quartz. (Fig. 4a)		U-Pb Zircon, this study
BD-1	11°34′ 01″N	92°44′ 10″E	South Andaman	Plagiogranite	Dominantly composed of plagioclase (commonly saussuritized) and quartz, with hypidiomorphic granular texture as described by Jafri et al. (1995). Minor amounts of amphibole, epidote and chlorite are also present (Fig. 4b). Smaller plagioclase grains appear to be floating between relatively larger quartz grains. Interstitial vermicular and micrographic intergrowths of quartz and plagioclase feldspar are also noted.	Presumably eqivalent with plagiogranites as reported by Jafri et al. (1995)	Presumably eqivalent with U-Pb Zircon, Sarma et al. (2010)
SA-GAB1	11°31′ 57″N	92°43′ 25″E	South Andaman	Layered gabbro	Interlayered gabbroic rock composed of olivine, plagioclase, clinopyroxene and minor amount of opaque minerals with a cumulate texture. Modal variation in plagioclase and olivine demarcate the layering (Fig. 4c). Two types of plagioclase grains - fresh and relatively altered (saussuritized) might be indicative of melt impregnation, as found in olivine rich troctolite in a nearby location (Ghosh et al., 2014). Amphibole is present along the olivine and plagioclase interface.		U-Pb Zircon, this study [Samples SA-GAB1 and SA-GAB2, occur as boulders on the coast near location 2 (Kodiaghat section, south Andaman), where exactly similar lithology is reported in situ (Ghosh et al., 2014). This confirms that boulder samples like SA-GAB1 are not out of context hence we consider them to be representative of in-situ samples.]
SA-GAB2	11°31′ 57″N	92°43′ 25″E	South Andaman	Cumulate interlayered rock (clinopyroxenite layers are surrounded by wehrlite on either side)	Clinopyroxene is almost exclusively present in the clinopyroxenite layer (Fig. 4d). Olivine grains are mostly altered (chlorite?) and almost absent in the clinopyroxenite layer and dominated in wehrlite layers. Minor proportion of plagioclase occur interstitially.		
CH-3	11°29′ 33″N	92°42′ 18″E	South Andaman	Plagiogranite clast	Plagiogranite clast, collected from the agglomerate, with hypidiomorphic granular texture. Composed of subequal proportions of quartz and plagioclase with minor proportions of epidote (Fig. 4e).		Presumably eqivalent with U-Pb Zircon, Pedersen et al. (2010)
CH-4	11°29′ 33″N	92°42′ 18″E	South Andaman	Pyroclastic (agglomerate)	Pyroclastic rock made of multiple rock fragments within an andesitic matrix composed of fine-grained plagioclase laths, epidote and a minor amount of pyroxene. The clasts include epidote rich clasts (epidosites?), andesite-dacite clasts (finer grained than the matrix) and leucocratic tonalite-plagiogranite clasts (Fig. 4f,g).		
AN1701	11°29′ 35″N	92°42′ 21″E	South Andaman	Pyroclastic (agglomerate)	Pyroclastic rock made of multiple litho fragments in a volcanic matrix. Amongst the fragments we have documented (i) a coarse grained plutonic quartzo-feldspathic rocks (plagiogranite) composed of saussuritized plagioclase, rare intergranular pyroxenes, and late stage epidote with a few opaque minerals, zircon and titanite. Some plagiogranite clasts show graphic intergrowth of quartz and feldspar; (ii) a coarse-grained plagioclase amphibole (along with minor opaque) bearing plutonic rock that could be a former gabbro/dolerite? (iii) a fine grained plagioclase and pyroxene bearing rock which dominates the clast proportion. We found chlorite to replace the former volcanic matrix suggesting some clasts could be andesite; (iv) large clinopyroxene fragment among other ophiolitic lithotypes (Fig. 4h,i).		

(continued on next page)

Table 1 (*continued*)

Sample	Coordinate		Island	Rock type	Petrographic feature	Geochemistry	Geochronogy
AN1719a	11°29′ 35″N	92°42′ 21″E	South Andaman	Tuff	Dacitic tuff (?) containing various litho-fragments including coexixting quartz and plagioclase. The plagioclase needles are aligned in places. We also note the presence of minor epidote, carbonate and opaque minerals.		
AN1720	11°29′ 43″N	92°42′ 18″E	South Andaman	Rhyolitic tuff	Volcanic rock with a fine-grained matrix containing rounded quartz, plagioclase and aggregates of epidote.		
AN1721a	11°29′ 59″N	92°42′ 18″E	South Andaman	Andesite	andesitic flow (?). This sample is made of fragments of variable size and a sub-volcanic andesitic nature floating in an isotropic brownish matrix.	this study	
AN1721b	11°29′ 59″N	92°42′ 18″E	South Andaman	Brecciated rhyodacite	The matrix is very fine grained, mainly made of small needles of plagioclase. Phenocrysts of quartz and plagioclase along with fragment of plagiogranite, rare epidote and chlorite to growth late (Fig. 4j).	this study	
AN1722b	11°29′ 59″N	92°42′ 18″E	South Andaman	Andesite	Volcanic rock made of plagioclase needles intergrown with amphibole almost without matrix. The texture suggests initial brecciation, possibly due to late stage hydrothermalism (Fig. 4k).	this study	
L-18	12°34′ 45″N	92°57′ 41″E	Middle Andaman	Leucocratic rock belonging to the diorite – granodiorite series	Leucocratic rock shows a hypidiomorphic granular texture and is dominantly composed of plagioclase and amphibole. From the textural perspective amphibole appears to be primary and sometimes replaced by chlorite (Fig. 4l).		U-Pb Zircon, this study
AN1703	12°35′ 44″N	92°57′ 27″E	Middle Andaman	Meta-chert (?)	Identified as representative of the metamorphic sole (sample AN1709a,b from	this study	
AN1704a	12°35′ 27″N	92°57′ 28″E		Amphibolite (meta-volcanics)	in-situ exposure of this metamorphic sole rock). Detailed petrographic descriptions of	this study	Ar-Ar Amphiobole, Plunder et al. (2020)
AN1709a	12°33′ 44″N	92°58′ 07″E			these samples are given in Plunder et al. (2020). Sample AN1703 is a quartz rich rock	this study	Ar-Ar Amphiobole, Plunder et al. (2020)
AN1709b	12°33′ 44″N	92°58′ 07″E			showing a mild foliation marked by green amphibole. Sample AN1713a is a mafic rock	this study	
AN1713a	12°35′ 16″N	92°57′ 34″E			with a nematoblastic texture. It is mainly made of amphibole and plagioclase.	this study	
AN1705a	12°32′ 26″N	92°58′ 31″E	Middle Andaman	Andesite-basaltic andesite	Volcanic rock, with altered plagioclase (sometimes with zoning pattern still visible) and chlorite rich pseudomorphs after clinopyroxene. The matrix is made of very fine-grained minerals that we identified as chlorite under the microscope and that replace a former glassy matrix. (Fig. 4m).	this study	
AN1705b	12°32′ 26″N	92°58′ 31″E	Middle Andaman	Andesite-basaltic andesite	Volcanic rock mainly made of plagioclase and pyroxene (now altered). In the former pyroxene we observed fine grained phyllosilicate that could be either chlorite or serpentine. Almost no matrix is present in between the grains. We also observed a few fragments of exotic rocks containing carbonate, quartz and serpentinite, possibly ophicalcite.	this study	
AN1705c	12°32′ 26″N	92°58′ 31″E	Middle Andaman	Andesite-basaltic andesite	Volcanic rock with plagioclase phenocrysts, and some grains totally replaced by a mixture of quartz and carbonate. We interpret them to be former pyroxene due to the presence of a former longitudinal cleavages and the shape. The matrix is very fine grained, made of small plagioclase crystals and a former glassy matrix. Some opaque minerals complete the assemblage.	This study	
AN1710a	12°34′ 21″N	92°57′ 50″E	Middle Andaman	Andesite-basaltic andesite	Volcanic rock consists of plagioclase phenocrysts, and some pseudomorphs in a fine-grained matrix. As in sample AN1705c we interpret these minerals as pseudomorphs after pyroxene (Fig. 4n).	This study	

Table 1 (*continued*)

Sample	Coordinate		Island	Rock type	Petrographic feature	Geochemistry	Geochronogy
AN1710c	12°34′ 21″N	92°57′ 50″E	Middle Andaman	Andesite-basaltic andesite	Volcanic rock with a fine-grained matrix that is now mainly made of chlorite and opaque mineral. The rock is highly oxidized and contains phenocryst of plagioclase and of former pyroxene that are replaced by a mixture of carbonate and chlorite. There are also late veins of carbonates (Fig. 4o).	This study	
AN1711	12°35′ 03″N	92°57′ 42″E	Middle Andaman	Andesite-basaltic andesite	Volcanic rock made of a fine-grained ground mass. The matrix is mainly made of plagioclase and pyroxene now mostly replaced by chlorite. Porphyroblasts are plagioclase (up to 5 mm) and clinopyroxene. There are many vacuoles filled with nice rosette-shaped chlorite and opaque minerals. Late veins of carbonate crosscut the rock (Fig. 4p).	This study	

contents of three Al_2O_3 rich samples (AN1705a, AN1705b, AN1710a) might reflect elemental mobility, although clustered SiO_2 and uncorrelated LOI contents do not support the hypothesis. Mg# are variable, ranging from 0.52 to 0.71 (Fig. 5d), and do not correlate with equally variable Cr and Ni contents of 20–580 ppm (Fig. 5e) and 30–250 ppm (Fig. 5f) respectively.

5.1.2. Trace elements

In the immobile element-based Total Alkali-Silica (TAS) proxy diagram (from Pearce, 2014, modified after Floyd and Winchester, 1975), which uses Nb/Y as a proxy for total alkalis ($Na_2O + K_2O$) and Zr/Ti as a proxy for SiO_2, all the amphibolite samples fall in or very close to the basalt field (Fig. 6a). Agglomerates samples from Middle and South Andaman fall in the basalt to andesite, basaltic andesite field, except for sample AN1721b, which falls in the rhyolite-dacite field, again consistent with petrographic observation.

To characterize our volcanic rocks in a more effective manner, we plot the obtained geochemical dataset in a N-MORB (Sun and McDonough, 1989) normalized spider diagram where the elements are ordered according to their average incompatibility during mantle melting, which efficiently distinguishes subduction influenced volcanic rocks (i.e. arc origin) from uninfluenced (i.e. MORB; Pearce, 2014; Fig. 6b-d).

All metamorphic sole samples except AN1704a have subparallel patterns and are enriched between 0.8 and 4 times relative to MORB. These samples show no HREE fractionation (flat patterns), are slightly enriched in light rare earth elements (LREEs) and show slight negative Nb, Ta, Hf, Zr and Ti anomalies. Sample AN1704a is more depleted in HREEs and more enriched in LREEs and shows more pronounced negative anomalies (Fig. 6b).

Agglomerates in Middle Andaman show both HREE and LREE fractionation, being depleted in HREEs and enriched in LREEs relative to MORBs. They show pronounced negative Nb, Ta, and Ti anomalies and slight Zr–Hf anomalies ranging from positive for the more fractionated samples to negative for the less fractionated ones (Fig. 6c). Sample AN1705c shows stronger LREE enrichment than the rest.

Agglomerates from South Andaman show patterns that are similar to those of volcanics of Middle Andaman and AN1704a (metamorphic sole) with fractionated LREE and HREE patterns and strong Nb–Ti negative anomalies. The Ta content was systematically below the 0.01 ppm detection limit. Out of three analysed samples only AN1721b has undepleted HREEs that are enriched from 0.8 to 2 times NMORB, slightly fractionated LREE enriched as much as 4 times NMORB, and have very pronounced Nb–Ti negative anomalies, as well as slight negative Zr–Hf anomalies (Fig. 6d). The contrasting composition of the volcanic rocks is also represented in the chondrite normalized (Sun and McDonough, 1989) REE multi-element spidergram (Fig. 6e-g). Middle Andaman sole samples show an almost flat REE pattern (except AN1704a). Agglomerates from middle and South Andaman (and AN1704a) are generally characterized by strong LREE enrichment and HREE depletion (Fig. 6e-g). We conclude from the above that the protolith of the metamorphic sole (except AN1704a) possesses distinct geochemical characteristics (no HREE fractionation, slightly more LREE-enriched than NMORB, slight negative Nb-Ta-Zr-Hf-Ti anomalies) with respect to the samples from the Middle and South Andaman agglomerates. Samples of Middle and South Andaman agglomerates have a general fractionated HREE pattern and strong negative Nb-Ta-Ti anomalies similar to that of metamorphic sole sample AN1704a.

5.2. Geochronology

Only a few zircon grains were recovered from gabbro sample SA-GAB1. Three short prismatic grains and one tip (grains 1–4, Supplementary Fig. 1) were analysed yielding variable $^{206}Pb/^{238}U$ ages between about 105 and 98 Ma (Table 3, Fig. 7). The pattern can in principle be explained by variable Pb loss of 105 Ma zircon, but this seems unlikely as the grains were of good quality and were chemically abraded, which commonly removes disturbed domains quite efficiently. The alternative is the presence of more than one generation. This interpretation implies that the youngest date of 98.56 ± 0.33 Ma is a maximum, and possibly the real age for emplacement of the gabbro. We consider 105 Ma the age of an older component picked up at the latest stage of magmatism or melting of pre-existing gabbroic crust. The larger error of the 105 Ma date is a function of the limited amount of Pb (and U) present in that grain. This suggests here were two different magmatic events that occurred around 98 and 105 Ma.

Plagiogranite sample 148A contains an abundant population of equant to prismatic zircon (Supplementary Fig. 1). Four analyses show a slight scatter yielding an average $^{206}Pb/^{238}U$ age of 98.74 ± 0.32 Ma dating emplacement. Zircon in plagiogranite L-18 occurs mostly as irregular, subsequent, anhedral grains and fragments, only partly showing euhedral faces or complete crystals (Supplementary Fig. 1). The four analyses overlap giving an average $^{206}Pb/^{238}U$ age of 93.48 ± 0.10 Ma dating magmatic crystallization.

6. Geochemical synthesis – Methods and limitations

6.1. Geochemical characterization of volcanic rocks of Andaman ophiolite

To resolve the debate on the geodynamic origin of the volcanic rocks, an extensive dataset has been compiled from the existing literature on Andaman and Nicobar Islands (Ghosh et al., 2017). Preliminary geochemical analyses of Ghosh et al. (2017) clearly revealed the potential of such a comparative study in explaining the varied geochemical

Table 2
Bulk rock geochemistry of selected samples of volcanic rocks and amphibolites from Andaman ophiolites.

Stratigraphy	Meta-chert (?)	Amphibolite (meta-volcanics)				Volcanic rock								
Sample No	AN1703	AN1704a	AN1709a	AN1709b	AN1713a	AN1705a	AN1705b	AN1705c	AN1710a	AN1710c	AN1711	AN1721a	AN1721b	AN1722b
Latitude	12°35′44″N	12°35′ 27″N	12°33′ 44″N	12°33′ 44″N	12°35′ 16″N	12°32′ 25″N	12°32′ 25″N	12°32′ 25″N	12°34′ 21″N	12°34′ 21″N	12°35′ 03″N	11°29′ 59″N	11°29′ 59″N	11°25′ 29″N
Longitude	92°57′27″E	92°57′ 28″E	92°58′ 07″E	92°58′ 07″E	92°57′ 34″E	92°58′ 37″E	92°58′ 37″E	92°58′ 37″E	92°57′ 50″E	92°57′ 50″E	92°57′ 42″E	92°42′ 18″E	92°42′ 18″E	92°36′ 28″E
Island	Middle Andaman											South Andaman		
SiO_2	90.46	58.84	52.83	52.03	50.65	57.44	55.51	57.69	56.08	53.42	52.78	54.70	78.89	58.09
TiO_2	0.11	0.48	1.31	1.39	1.52	0.72	0.94	0.77	1.03	0.63	0.76	0.73	0.27	1.01
Al_2O_3	3.17	13.35	13.67	14.29	13.59	18.84	18.74	16.31	19.88	16.17	19.05	15.14	11.35	14.82
Fe_2O_3[†]	0.37	0.99	1.66	1.68	1.82	1.21	1.34	1.09	1.15	1.36	1.54	1.48	0.36	1.39
FeO[†]	1.90	5.06	8.45	8.55	9.29	6.16	6.86	5.58	5.84	6.91	7.86	7.56	1.85	7.09
MnO	0.06	0.16	0.20	0.19	0.26	0.13	0.12	0.20	0.04	0.36	0.18	0.13	0.02	0.16
MgO	1.12	7.18	7.83	8.08	8.26	6.91	8.81	4.20	8.07	5.37	4.79	6.93	0.39	6.16
CaO	1.34	7.04	9.09	9.05	10.03	0.52	0.54	6.10	0.58	9.13	6.39	8.51	1.18	4.88
Na_2O	1.21	5.07	4.05	3.69	3.18	7.33	6.25	7.46	6.98	6.25	6.29	4.58	5.58	6.08
K_2O	0.18	1.72	0.80	0.90	1.22	0.56	0.69	0.31	0.18	0.12	0.24	0.09	0.09	0.20
P_2O_5	0.06	0.12	0.12	0.15	0.19	0.19	0.20	0.26	0.18	0.28	0.13	0.14	0.03	0.13
Total[**]	100.00	100.00	100.00	100.00	100.00	100.00	100.00	100.00	100.00	100.00	100.00	100.00	100.00	100.00
Mg#	0.51	0.72	0.62	0.63	0.61	0.67	0.70	0.57	0.71	0.58	0.52	0.62	0.27	0.61
LOI	0.27	0.9	1.31	2.16	1.25	4.56	6.24	6.82	6	10.35	5.43	3.47	1.04	2.95
Total (original)	99.28	99.94	100.2	100.8	100.8	100.2	100.1	100.2	99.92	100.4	100.3	99.38	99.87	100.4
Sc	5	17	42	40	38	16	37	25	16	22	35	35	10	32
V	36	101	302	294	287	162	227	205	168	142	267	266	17	295
Cr	<20	410	170	280	280	40	240	110	580	130	60	40	< 20	20
Co	11	31	40	41	47	23	31	16	42	22	26	26	3	27
Ni	20	280	80	100	170	50	80	50	250	80	30	30	< 20	30
Cu	10	40	50	40	90	80	100	30	90	40	90	40	10	30
Zn	<30	80	80	90	90	80	70	60	160	40	90	< 30	< 30	< 30
Ga	3	11	15	16	13	13	15	12	17	10	12	15	10	13
Rb	3	24	9	14	15	9	10	4	4	3	3	< 1	< 1	2
Sr	45	55	164	110	223	363	289	422	162	177	436	140	101	172
Y	5.9	19.5	29.2	27.9	34.3	19.4	15.8	26	14.1	14.4	18.2	17.3	41.1	19.3
Zr	21	55	75	83	93	115	68	181	71	63	46	55	134	67
Nb	<0.2	3.5	3.4	4.7	2.7	3.5	2	3.1	2.3	1.6	0.4	0.4	1.2	0.6
Cs	<0.1	<0.1	0.1	0.1	<0.1	0.3	0.3	<0.1	0.3	0.2	<0.1	<0.1	<0.1	<0.1
Ba	60	124	217	188	582	403	398	297	186	127	174	14	21	64
La	6.67	17.5	4.51	5.76	5.99	5.35	4.4	17.2	4.02	5.3	4.32	5.47	9.57	3.8
Ce	15.1	29.8	11.8	14.3	14.7	13.3	10.9	39.2	9.71	11.9	10.4	15	24.5	9.94
Pr	1.58	4.28	1.82	2.09	2.29	1.92	1.62	5.05	1.52	1.58	1.69	2.46	3.55	1.62
Nd	6.65	18.2	9.33	10.8	11.6	8.65	7.61	20.9	7.44	7.55	8.15	11.7	16.8	8.07
Sm	1.46	4.02	3.09	3.52	3.82	2.49	2.07	4.67	2.24	2.2	2.35	3.11	4.72	2.5
Eu	0.336	0.895	1.15	1.3	1.32	0.714	0.644	1.33	0.636	0.82	0.803	0.993	1.19	0.86
Gd	1.36	3.94	4.31	4.72	5.12	2.9	2.48	4.58	2.72	2.77	2.87	3.34	5.71	3.12
Tb	0.22	0.62	0.77	0.79	0.92	0.52	0.45	0.75	0.43	0.44	0.51	0.52	1.02	0.54
Dy	1.25	3.54	5.3	5	5.99	3.35	2.77	4.65	2.63	2.59	3.34	3.17	6.62	3.62
Ho	0.22	0.66	1.05	1.05	1.26	0.7	0.56	0.92	0.54	0.51	0.64	0.62	1.35	0.68
Er	0.6	1.92	3.12	2.94	3.64	2	1.65	2.59	1.63	1.45	1.93	1.75	4.4	1.97
Tm	0.08	0.288	0.448	0.422	0.565	0.286	0.23	0.367	0.238	0.196	0.292	0.275	0.68	0.293
Yb	0.51	1.77	2.96	2.74	3.93	1.92	1.52	2.42	1.59	1.21	2	1.76	4.74	2.02
Lu	0.08	0.264	0.445	0.429	0.618	0.304	0.244	0.374	0.255	0.185	0.305	0.259	0.749	0.31
Hf	0.5	1.6	2.1	2.1	2.2	2.5	1.8	4.1	1.8	1.6	1.3	1.6	3.6	1.8
Ta	<0.01	0.25	0.2	0.3	0.11	0.19	0.27	0.16	0.04	0.02	<0.01	<0.01	<0.01	<0.01
Pb	<5	6	< 5	< 5	5	< 5	6	7	<5	<5	<5	<5	<5	6
Th	1.18	3.04	0.38	0.51	0.39	2.23	0.65	6.3	0.78	0.84	0.53	0.59	1.17	0.33
U	0.1	0.74	0.12	0.14	0.22	0.9	0.38	1.29	0.33	0.32	0.2	0.18	0.33	0.12

[†] FeO and Fe_2O_3 are adjusted as per $Fe^{2+}/Fe_{tot} = 0.85$ (eg. Schilling et al., 1983).
[**] Total indicates oxides recalculated on an anhydrous basis,original total is also given.

spectrum of volcanics in a supra-subduction zone environment. Comparison of our new results with the previously published data provides comprehensive insights into the geochemical variability of the Andaman Nicobar volcanic rocks and their relation to the mantle rocks. To this end, we included our geochemical results of agglomerates, of sole (from location 1 and 6) and of two previously published dataset (Pedersen et al., 2010; Sachin et al., 2017) into the compilation of Ghosh et al. (2017) (Supplementary Table 2). Please note the lower lava and upper lava (as well as pillow basalt and east coast volcanics) distinction was followed after Ghosh et al. (2017, for details see table 7.2). The data sets of Sachin et al. (2017) and Jafri and Sheikh (2013) are from Great Nicobar and Bompoka Island, respectively (See Fig. 1a for location). From field, petrographic and geochemical perspective, the agglomerates from South and Middle Andaman are found to possess more or less similar characteristics and thus considered as a single group in our synthesis. The corresponding major element plots of the compiled dataset are given as overlay in Fig. 5. Variable and sometimes substantial LOI values have been reported for volcanic rocks, highlighting the possibility of element mobility. For this reason, and because Ghosh et al. (2017) have already attempted a geochemical characterization of the Andaman and Nicobar Islands volcanic rocks based on major elements, we herein focus on trace elements that are deemed immobile in ophiolitic environments and show a better potential to accurately discriminate tectonic affinities (Dilek and Furnes, 2011; Pearce, 2014).

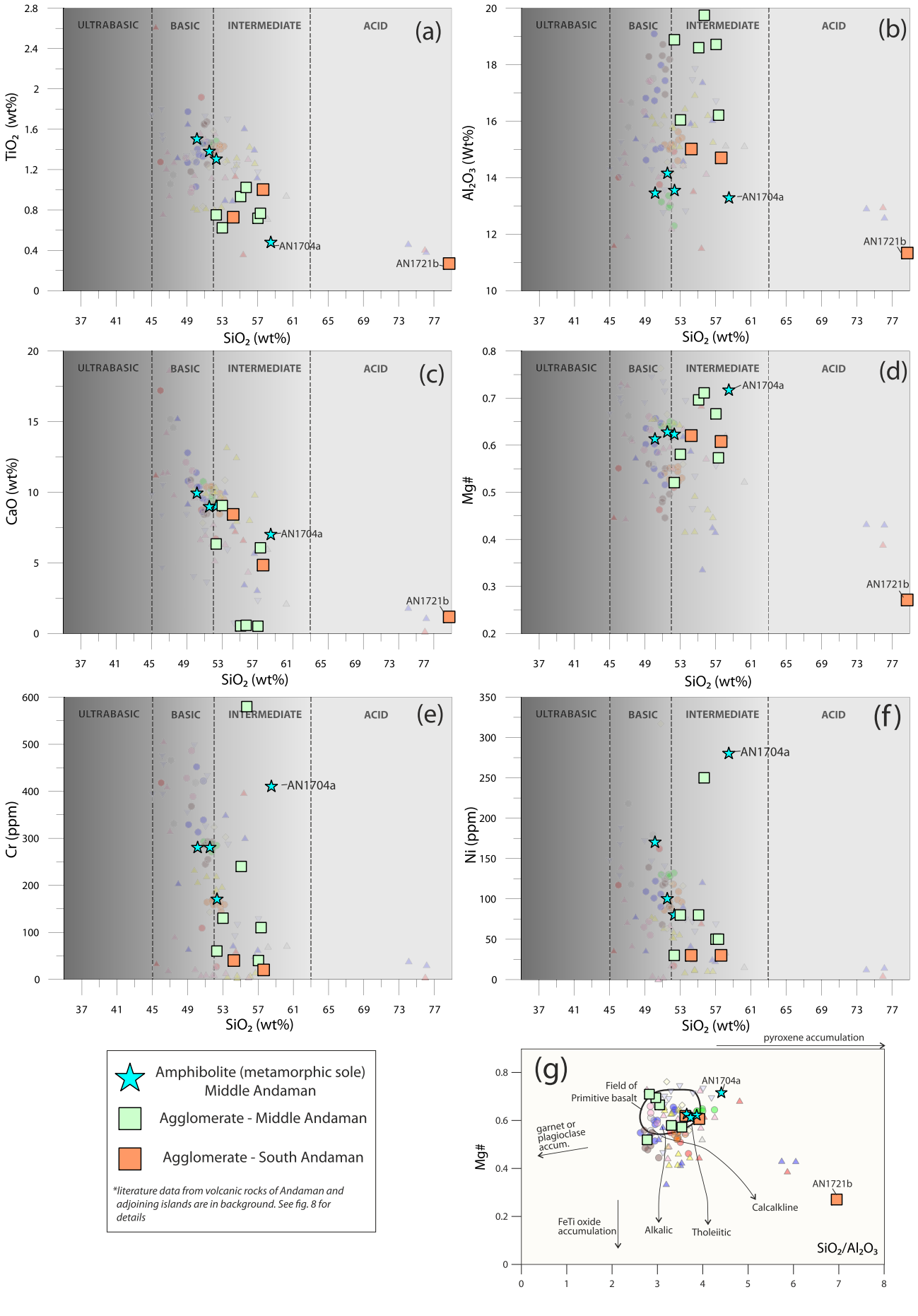
(a)
ULTRABASIC
BASIC
INTERMEDIATE
ACID
TiO2 (wt%)
SiO2 (wt%)
AN1704a
AN1721b
(b)
Al2O3 (Wt%)
(c)
CaO (wt%)
(d)
Mg#
(e)
Cr (ppm)
(f)
Ni (ppm)
Amphibolite (metamorphic sole) Middle Andaman
Agglomerate - Middle Andaman
Agglomerate - South Andaman
*literature data from volcanic rocks of Andaman and adjoining islands are in background. See fig. 8 for details
(g)
pyroxene accumulation
Field of Primitive basalt
garnet or plagioclase accum.
FeTi oxide accumulation
Alkalic
Tholeiitic
Calcalkline
SiO2/Al2O3

6.2. Geochemical modelling

Volcanic rocks are susceptible to post/syn extrusion alteration and fractionation, and thus inferring the correct parental melt chemistry is crucial to understand the genesis of the basalt in the source mantle. Although tricky, a reasonable estimate of a primary basalt could be achieved using: (1) a petrogenetic grid for mantle melting (e.g. PRIMELT2 model) (Herzberg and Asimow, 2008, and references therein); (2) thermodynamic phase equilibria model calculations (e.g. pMELTS; Ghiorso et al., 2002; Asimow et al., 2004); or (3) an iterative algorithm that allows to estimate primary basalt compositions using back calculations along the fractional crystallization path of a magma (e.g. PRIMACALC2, Excel based WINDOWS application software; Kimura and Ariskin, 2014). Apart from the estimation of major and trace element compositions of primary melts in a variety of tectonic settings, PRIMACALC2 is capable of calculating various important parameters related to source mantle conditions, like degree of melting and temperature and pressure of melting, which we consider an important proxy for correlating source mantle conditions with the observed geochemical diversity of the volcanic rocks in the Andaman ophiolite.

We could not get successful results for the entire dataset due to program specific limitations. Samples with low Ni (indicative of too much fractionation), or high Ni, due to Si-rich pyroxenite sources in arc basalts, resulting in high NiO in olivines, are outside the desired equilibrium field and hence excluded for further consideration. We had to exclude a few samples because they were deemed to be inappropriate for calculations in COMAGMAT3.72 (for details see Ariskin and Barmina, 2004, and references therein), a subsidiary program used in PRIMACALC2 for back-calculation. Another major problem is the significant amount of loss on ignition (LOI) (e.g. >4 wt%) in a number of samples. Being a compilation, we do not have the scope to judge the individual analytical techniques and we speculate that such variable amounts of LOI are indicative of extensive alteration and hence could be a potential source of error in estimating source conditions. Considering all these limitations, instead of drawing first order conclusions we use the obtained results as one of the complementary models to supplement our geochemical observations (Fig. 8) and as a basis of further discussion. For this study we use mantle melting temperatures and degree of melting obtained for the volcanic rocks to check the consistency of the geochemical observation (reported in Fig. 8 and Fig. 9a) and further correlate it with degree of mantle melting obtained from peridotite geochemistry.

To obtain the degree of mantle melting directly from the peridotite chemical composition we have performed numerical melting experiments via the alphaMELTS program (Smith and Asimow, 2005) with Depleted MORB Mantle (DMM; Workman and Hart, 2005) as starting material. Results (clinopyroxene composition) of near-fractional isentropic melting of DMM (up to ~14%, which is found to be maximum extent of the melting in the numerical experiment performed here) are shown in primitive mantle-normalized (McDonough and Sun, 1995) and chondrite normalized (Sun and McDonough Sun and McDonough, 1989) multi-element spidergrams (Fig. 9b and c, respectively).

7. Discussion

7.1. Contrasting geochemical characters of the Andaman ophiolite volcanic rocks – Tectonic discrimination

Owing to the different elemental property of Th (subduction-mobile) and Nb (subduction-immobile) in most arc systems Th/Nb is an ideal proxy for differentiating MORB lava from subduction-influenced ones (Pearce, 2008). Many of the analyses compiled from the literature do not include Th or Nb, therefore we interpret and compare our own samples with a restrained set of data. As suggested in Pearce (2014) we use this diagram in combination with the V/Ti diagram from Shervais (1982), which highlights the contribution of water to mantle melting. In the Th/Yb - Nb/Yb diagram (Pearce, 2008, 2014), pillow lavas from South Andaman (green circle, Jafri et al., 2010) and Bompoka Island (orange circle, Jafri and Sheikh, 2013) plot within the MORB-OIB array, having apparently been sourced from depleted MORB mantle (Fig. 8a). They also fall within the MORB or slab distal field of the V/Ti diagram (Fig. 8b), from which we infer that they represent basalts erupted from relatively shallow and dry melting of a depleted mantle source, corresponding to a mid-ocean ridge environment. Other reported analyses of "pillow basalt", sometimes referred as "Upper Lavas" units from Rutland, lack Th or Nb analyses, and plot in the MORB field of V/Ti diagram (Fig. 8b). These include: red circle, Bhattacharya et al. (2013), South Andaman; grey circle, Pal, 2011; brown circle, Jafri et al. (1990), based on location and authors' interpretation; pink circle, Srivastava et al. (2004), based on location and authors' interpretation; pale yellow diamond, Pedersen et al. (2010). The same characteristics also apply to basalts from Great Nicobar Islands (inverted pale blue triangle, Sachin et al., 2017).

Analyses of East Coast volcanics, also referred as "Lower Lavas", have geochemical characteristics that differ from the Pillow Basalt unit. In the Th/Yb - Nb/Yb diagram, East Coast volcanic rocks (yellow triangle, Ghosh et al., 2014) follow an intra-oceanic arc trend, parallel to the mantle array but significantly depleted in Nb (Fig. 8a). Other analyses compiled from the literature lack Nb and/or Th contents but were still plotted on the V–Ti diagram. Lower lava samples from Rutland (red triangle, Bhattacharya et al., 2013) and South Andaman (grey triangle, Pal, 2011; pink triangle, Srivastava et al., 2004, based on location and authors' interpretation) all straddle the Island Arc Tholeiite to MORB – slab distal fields. Interpreted together, such rocks likely resulted from melting of a re-fertilized depleted mantle in a water present environment, corresponding to an intra-oceanic arc or back-arc basin (Fig. 8b).

In the Th/Yb - Nb/Yb diagram, metamorphic sole samples (cyan star, except for AN1704a) plot near the mantle array, but with a slight slab component, as suggested by their negative Nb-Ta-Ti anomalies (Fig. 8a). They plot in the MORB-slab distal field of the V–Ti diagram (Fig. 8b). Considering the non-negligible Nb-Ta-Ti negative anomalies, we interpret the protolith of the metamorphic sole as a basaltic rock that resulted from partial melting of a depleted to enriched mantle source in the presence of low amounts of water and with a slight influence from a slab, which we interpret as a back-arc basin spreading centre. In the Th/Yb - Nb/Yb diagram, agglomerates from both South and Middle Andaman (neon red square) along with AN1704a (metamorphic sole) plot away from MORB-OIB array and thus clearly show subduction influence (Fig. 8a). South Andaman (AN1721a, AN1721b, AN1722b) and one Middle Andaman agglomerate (AN1711) samples show strong intra-oceanic arc signatures and appear to be sourced from an ultra-depleted mantle (Nb/Yb < 1). Amongst these samples, AN1721a (South Andaman) and AN1711 (Middle Andaman), plot in the Island Tholeiite field of the V–Ti diagram, consistent with melting in the presence of water (Fig. 8b). The geochemistry of these samples is akin to that of the East-Coast volcanics (reported by Ghosh et al., 2017, yellow triangle).

In the Ce/Nb - Th/Nb diagram (Saunders and Tarney, 1991), back-arc basin basalts tend to fall in the intermediate zone between the low Th/Nb zone (MORB-OIB) and high Th/Nb (Island Arc basalts) zone (Fig. 8c). Pillow lavas from South Andaman (green circle) have relatively high Ce/

Fig. 5. Bivariate plots (major and minor element based) of geochemical data from Middle and South Andaman volcanic rocks and amphibolites (Metamorphic sole) – (a) SiO_2 – TiO_2; (b) SiO_2 – Al_2O_3; (c) SiO_2 – CaO; (d) SiO_2 – Mg#; (e) SiO_2 – Cr; (f) SiO_2 – Ni; (g) SiO_2/Al_2O_3 – Mg# (after Kempton and Harmon, 1992); All data have been plotted on an anhydrous basis (Table 2). Compiled data of volcanic rocks (see Supplementary Table 2) from Andaman and neighbouring islands are shown as transparent overlays in background, to show the entire spectrum (for symbols see Fig. 8). The grey shades indicate the ultrabasic, basic, intermediate and acid boundaries (after Le Bas et al., 1986, Fig. 2).

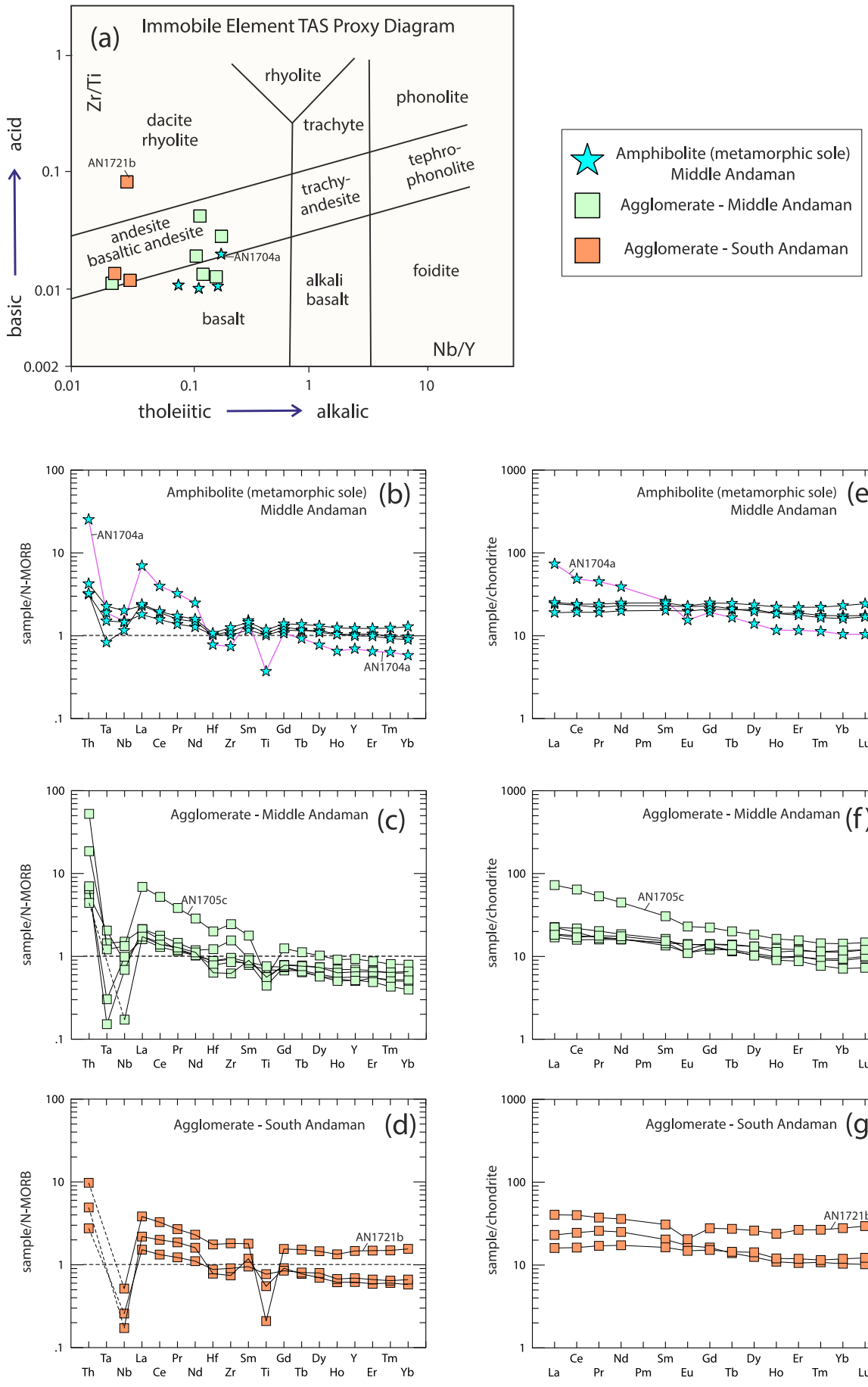
(a)
Immobile Element TAS Proxy Diagram
Zr/Ti
Nb/Y
rhyolite
phonolite
dacite
rhyolite
trachyte
tephro-
phonolite
trachy-
andesite
andesite
basaltic andesite
alkali
basalt
foidite
basalt
AN1721b
AN1704a
acid
basic
tholeiitic
alkalic
Amphibolite (metamorphic sole)
Middle Andaman
Agglomerate - Middle Andaman
Agglomerate - South Andaman
(b)
(c)
(d)
(e)
(f)
(g)
sample/N-MORB
sample/chondrite
AN1705c
Th Nb Ce Nd Zr Ti Tb Ho Er Yb
La Pr Pm Eu Tb Ho Tm Lu

Table 3
U–Pb data for zircon from Andaman samples.

Properties	Weight	U	Th/U	Pbc	206/204	207/235	2 sigma	206/238	2 sigma	rho	207/206	2 sigma	206/238	2 sigma	207/235	2 sigma
	[ug]	[ppm]		[pg]			[abs]		[abs]			[abs]	[Ma]	[abs]	[Ma]	[abs]
(a)	(b)	(b)	(c)	(d)	(e)	(f)	(f)	(f, g)	(f)	(f)	(f,g)	(f)	(f,g)	(f)	(f)	(f)
SA-GAB1: Layered gabbro, South Andaman (11°31′57″N / 92°43′25″E)																
1 - Z eu sp. [1]	1	44	1.06	1.4	51	0.10259	0.01344	0.016473	0.000213	0.21	0.04517	0.00583	105.32	1.35	99.16	12.30
2 - Z tip [1]	1	137	0.60	1.0	157	0.10303	0.00314	0.015689	0.000064	0.28	0.04763	0.00141	100.35	0.41	99.57	2.89
3 - Z eu sp. [1]	1	124	0.85	0.9	156	0.10475	0.00344	0.015589	0.000063	0.33	0.04873	0.00155	99.72	0.40	101.15	3.16
4 - Z eu sp. [1]	2	68	0.68	0.7	210	0.10019	0.00266	0.015407	0.000051	0.37	0.04717	0.00120	98.56	0.33	96.96	2.45
148A: Plagiogranite, Rutland Island (11°24′10″N / 92°39′34″E)																
5 - Z eu sp. [3]	20	68	0.72	1.4	955	0.10246	0.00060	0.015473	0.000035	0.48	0.04803	0.00025	98.98	0.22	99.05	0.56
6 - Z eu lp [6]	22	91	0.65	0.7	2739	0.10195	0.00036	0.015436	0.000034	0.71	0.04790	0.00012	98.74	0.22	98.58	0.33
7 - Z eu sp. [1]	18	87	0.36	1.1	1360	0.10149	0.00044	0.015435	0.000034	0.60	0.04769	0.00017	98.74	0.22	98.15	0.41
8 - Z eu eq-sp [12]	26	91	0.64	1.5	1499	0.10221	0.00042	0.015395	0.000034	0.64	0.04815	0.00015	98.49	0.22	98.81	0.38
L18: Leucocratic rock belonging to the diorite – granodiorite series, Middle Andaman (12°34′45″N / 92°57′41″E)																
9 - Z eu + fr [9]	33	364	1.03	1.5	7145	0.09700	0.00029	0.014616	0.000032	0.84	0.04813	0.00008	93.54	0.21	94.00	0.26
10 - Z fr [11]	27	308	1.09	0.8	9831	0.09662	0.00027	0.014615	0.000031	0.83	0.04795	0.00008	93.53	0.20	93.65	0.25
11 - Z eu [8]	22	467	0.97	3.1	2994	0.09665	0.00028	0.014608	0.000031	0.81	0.04799	0.00008	93.49	0.19	93.68	0.26
12 - Z fr [1]	38	395	0.99	1.2	11,202	0.09635	0.00026	0.014585	0.000031	0.89	0.04791	0.00006	93.34	0.20	93.40	0.24

a)Z = zircon; eu = euhedral; lp = long prismatic; sp. = short prismatic; eq = equant; fr = fragment; [n] = number of grains in fraction; all zircon treated with chemical abrasion (Mattinson, 2005).
b)Weight and concentrations are known to better than 10%.
c)Th/U model ratio inferred from 208/206 ratio and age of sample.
d)Pbc = total common Pb (initial + blank).
e)Raw data, corrected for fractionation and spike.
f)Corrected for fractionation, spike, blank (206/204 = 18.59; 207/204 = 15.55) and initial common Pb (based on Stacey and Kramers, 1975); error calculated by propagating the main sources of uncertainty; The U–Pb ratio of the spike used for this work is adapted to 206Pb/238 U = 0.015660 for the ET100 solution as obtained with the ET2535 spike at NIGL.
g)Corrected for 230Th disequilibrium according to Schärer (1984) and assuming Th/U magma = 4.

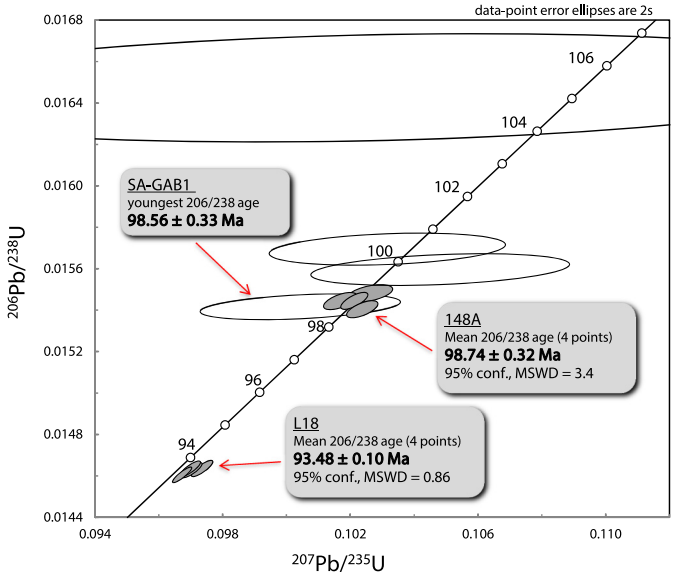

Fig. 7. Geochronological results - Concordia diagram for zircons recovered from sample SA-GAB1, 148A and L-18. Data point error ellipses are 2σ. See table 3.

Nb and low Th/Nb zone and plot near the N-MORB domain. Agglomerates and East Coast volcanics (yellow triangle) are characterized by high Ce/Nb and high Th/Nb typical of arc volcanics. Interestingly, sole samples plot in the intermediate zone and near to the back-arc basin basalts from the Mariana Trough (Fig. 8c). A similar intermediate Ce/Nb and Th/Nb ratio in pillow basalts from Bompoka Island (orange circle) indicates a back-arc origin. In the La/Nb - Y diagram (Floyd et al., 1991) sole samples along with pillow basalts from Bompoka Island fit in the BABB (back-arc basin basalts) field (Fig. 8d). Agglomerates and East Coast volcanics (Ghosh et al., 2014) are characterized by higher La/Nb ratio and mostly plot in fields of subduction influenced basalts – forearc platform basalts (FAPB) and IAT. All previous diagrams suggest a N-MORB affinity for pillow lavas from South Andaman (green circle), however their origin remains inconclusive in the La/Nb – Y diagram. Saccani

Fig. 6. Trace and REE geochemistry of Middle and South Andaman volcanic rocks and amphibolites (metamorphic sole). (a) Immobile element-based TAS (Total Alkali-Silica) proxy diagram (from Pearce, 2014, after Floyd and Winchester, 1975); (b-f) N-MORB and chondrite (Sun and McDonough, 1989) normalized spidergram, (b,e) amphibolites (Middle Andaman), (c,f) agglomerates (Middle Andaman) and (d,g) agglomerates (South Andaman).

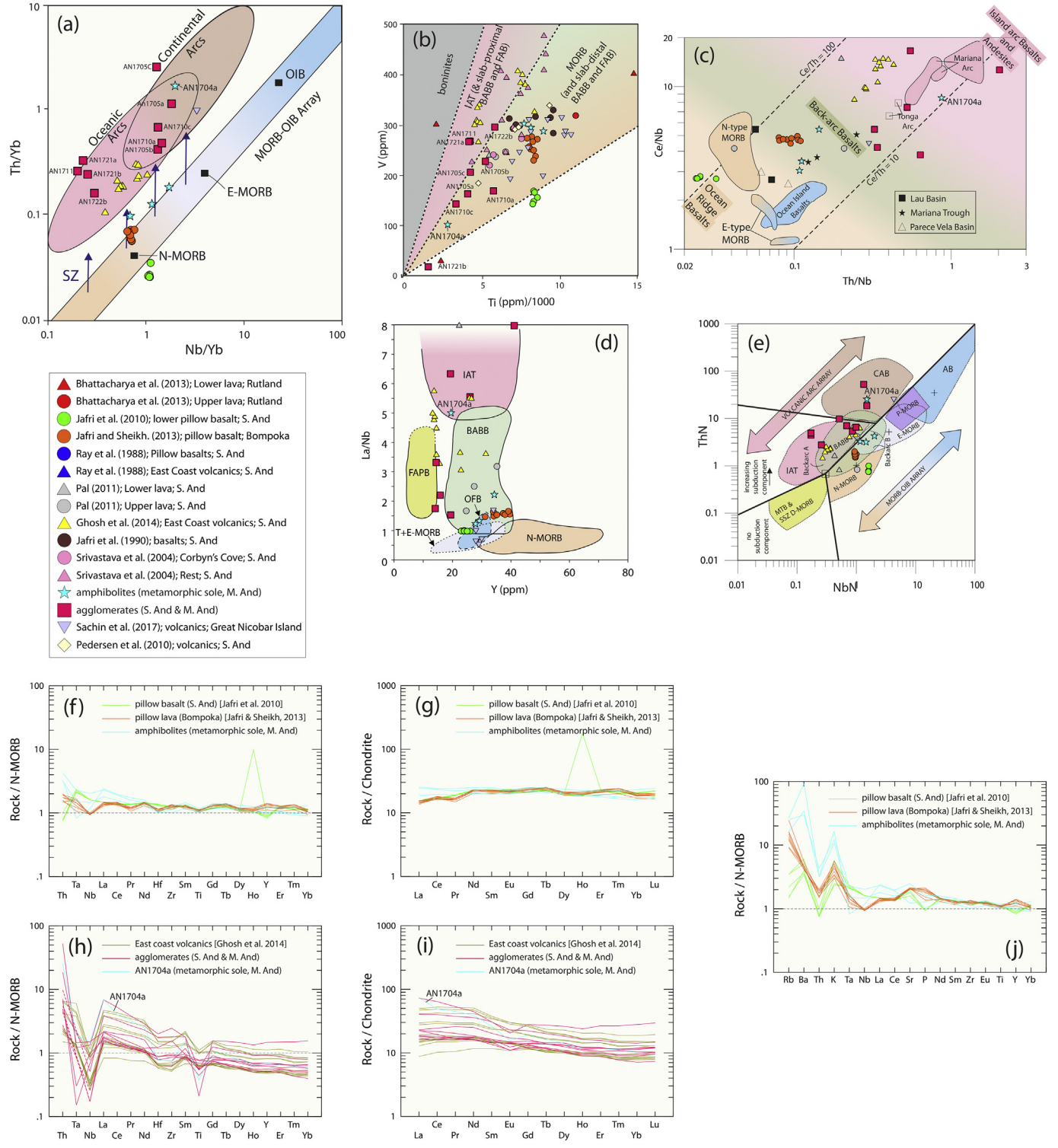

Fig. 8. Tectonic discrimination of volcanic rocks of Andaman ophiolite: (a) Th/Yb - Nb/Yb diagram (Pearce, 2008, 2014); (b) V - Ti diagram (Shervais, 1982); (c) Ce/Nb - Th/Nb diagram (Saunders and Tarney, 1991); (d) La/Nb - Y diagram (Floyd et al., 1991), (e) Th_N - Nb_N diagram (Saccani, 2015). N-MORB (f,h); (j) with emphasis on LILE, (g,i) chondrite normalized spidergram for volcanic rocks of Andaman ophiolite. OIB: ocean-island basalt; MORB: mid-ocean ridge basalt, N-: normal type, *E*-: enriched type, P-: plume type, D-: depleted type; MTB: medium-Ti basalt; IAT: island arc tholeiites; BABB: back-arc basin basalts; OFB: oceanic flood basalt; FAPB: forearc platform basalt; AB: alkaline basalt; CAB: calc-alkaline basalt. Data source with colour codes: red: Bhattacharya et al. (2013); yellow: Ghosh et al. (2014); orange: Jafri and Sheikh (2013); green: Jafri et al. (2010); brown: Jafri et al. (1990); blue: Ray et al. (1988); grey: Pal (2011); pink: Srivastava et al. (2004); light purple: Sachin et al. (2017); pale yellow: Pedersen et al. (2010); neon red: agglomerates (South and Middle Andaman, present study); cyan: metamorphic sole (present study). Details of data source and meaning of symbols are also given in the diagram.

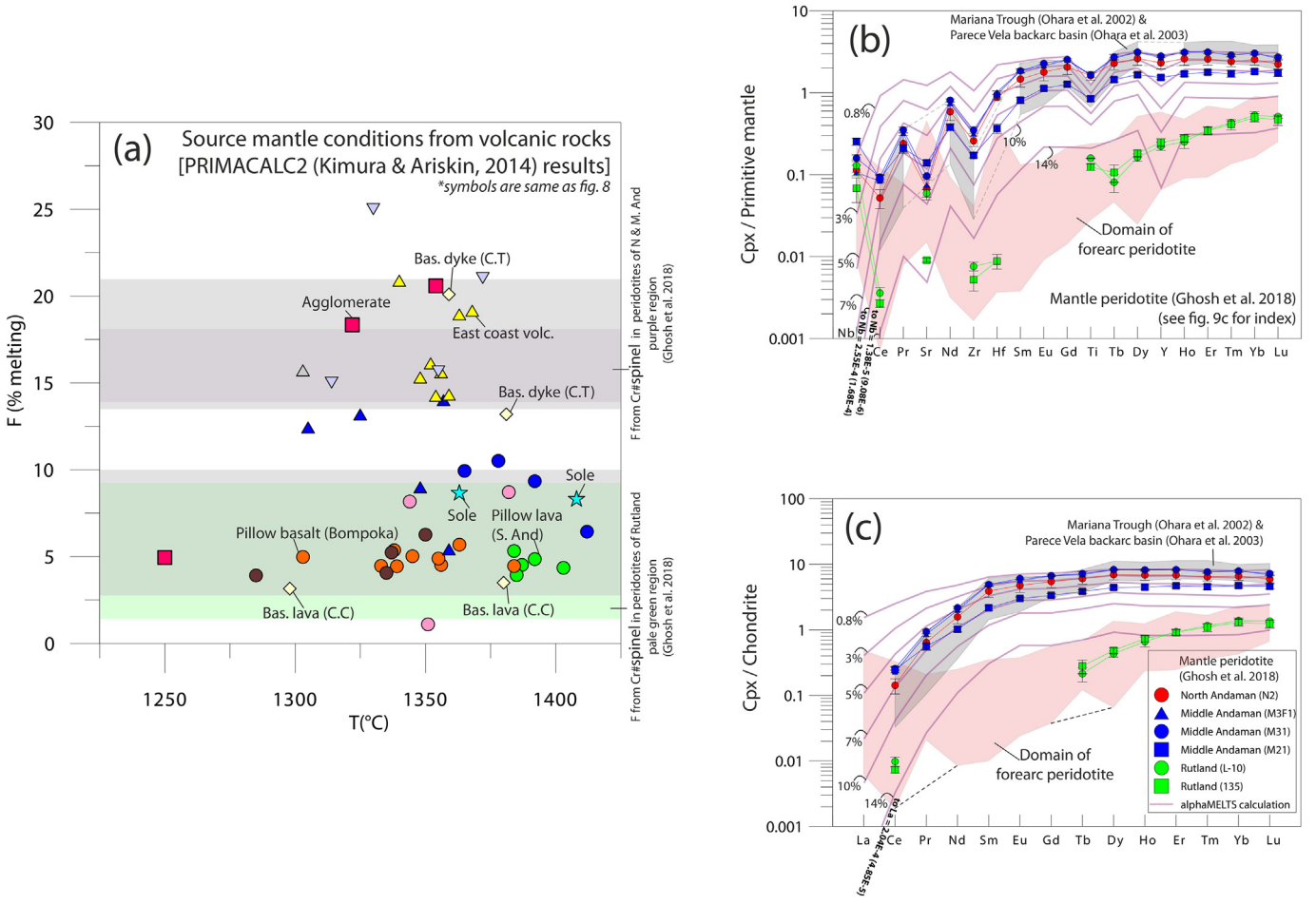

Fig. 9. (a) Source mantle conditions of volcanic rocks of Andaman ophiolite - Degree of melting vs Temperature diagrams (calculated using PRIMACALC2; Kimura and Ariskin, 2014). Degree of melting calculated from chrome spinel (Ghosh et al., 2018) is also shown. Pale green band: degree of melting from $Cr\#_{spinel}$ in peridotites of Rutland; purple band: degree of melting from $Cr\#_{spinel}$ in peridotites of North and Middle Andaman; symbols are the same as in Fig. 8; (b) primitive mantle; (c) chondrite normalized plot REE patterns of clinopyroxene of the DMM (Workman and Hart, 2005) after melting calculation (using alphaMELTS program, Smith and Asimow, 2005, see text for details, degree of melting are shown in %). Clinopyroxene trace element patterns of Rutland, North and Middle Andaman peridotite (Ghosh et al., 2018) along with the domain of back-arc peridotite (Ohara et al., 2002, 2003) and forearc peridotites (compiled in this study, see Supplementary Fig. 3) are also shown. Owing to extremely low values (normalized) for Nb (in Fig. 9b) and La (in Fig. 9c), numeric values are mentioned in the respective diagrams (original in parentheses).

(2015) proposed a new discrimination diagram using absolute measures of Th and Nb based on >2000 known ophiolitic basalts and ~ 560 modern rocks from known tectonic settings. In the Th_N - Nb_N diagram (Fig. 8e; Nb and Th normalized with respect to N-MORB) we can see a clear distinction between two groups of volcanic rocks of the Andaman Islands. Pillow lavas from South Andaman (green circle), Bompoka Island (orange circle) and sole samples plot in the domain of no subduction component. Contrastingly, agglomerates, AN1704a (sole) and East Coast volcanics (yellow triangle) are in the subduction-influenced domain. Furthermore, the BABB field overlaps with various volcanic rocks (IAT, CAB, N-MORB, *E*-MORB) and is further subdivided as back-arc A and back-arc B domains. Back-arc A indicates BABB characterized by input of subduction or crustal components (e.g. immature intra-oceanic or ensialic back-arc), whereas back-arc B indicates BABB with no input of subduction or crustal components (e.g. mature intra-oceanic back-arc). Hence, from Fig. 8e we can conclude that agglomerates, AN1704a (sole) and East Coast volcanics (Ghosh et al., 2014) probably formed in an arc – arc proximal back-arc environment whereas sole samples, along with pillow basalts from Bompoka Island (Jafri and Sheikh, 2013) with MORB affinity, represent volcanics of a slab distal back-arc setting.

The sharp geochemical contrast of the two groups of volcanic rocks has been clearly distinguished in these diagrams and further substantiated by the multielement N-MORB and chondrite (Sun and McDonough, 1989) normalized spidergram. In most cases the full suite of trace and rare-earth elements is missing, but wherever available the data are plotted (Supplementary Fig. 2a-r). We found three datasets of volcanic rocks with the nearly complete spectrum as summarized in Fig. 8f-i. In the N-MORB normalized diagram, sole samples (except AN1704a) plot very close to N-MORB (especially in REEs) and display a very similar character to that of pillow lavas from South Andaman and Bompoka Island. However, the slight negative Nb, Ta, Hf, Zr and Ti anomalies of the metamorphic sole are almost absent in South Andaman pillow basalts and very subtle in Bompoka pillow basalts (Fig. 8f). The variable Nb-Ta-Ti anomalies, ranging from obvious (AN1704a) to negligible (AN1709a), point towards a back-arc setting with variable slab influence whereas pillow basalts are expected to form by a high degree of partial melting of a depleted mantle source at shallow depth, typical of mid ocean ridge. Owing to the presence of a slight Ti anomaly in the pillow basalts the possibility of the presence of a slab distal component (BABB) cannot be ruled out. The chondrite normalized diagram (Fig. 8g) for the same group of samples shows very flat REE patterns. Agglomerate samples (and AN1704a) show a contrasting geochemical behaviour to that of the sole samples (discussed in the section 5.1.2) and are near identical with the East Coast volcanics (Ghosh et al., 2014) except that the later show Ta

enrichment with respect to Nb (Fig. 8h,i). Sole samples (except AN1704a), pillow lavas from South Andaman and Bompoka Island have been previously seen to have a geochemical character very close to N-MORB (Fig. 8a,f,g), however, in the large ion lithophile element (LILE) bearing N-MORB normalized spidergram all three datasets - sole samples, pillow lavas from South Andaman and Bompoka Island - display a significant enrichment of Rb, Ba, K, Sr (Fig. 8j). Enrichment of LILE in back-arc basin basalts has been previously documented by Saunders and Tarney (1991). Such LILE enrichment of pillow basalts from South Andaman and Bompoka Island has been proposed to be indicative of back-arc basin basalt affinity (Jafri et al., 2010; Jafri and Sheikh, 2013). A similar inference could be made for the metamorphic sole, but the robustness of such an interpretation could be questioned since trace elements in these rocks, especially the LILE, are prone to have been significantly modified during metamorphism (Ishikawa et al., 2005).

The results obtained by PRIMACALC2 (Fig. 9a) also clearly demonstrate that the volcanics with arc affinity, agglomerates, East Coast volcanics (Ghosh et al., 2014; Ray et al., 1988), and a few samples from Great Nicobar (Sachin et al., 2017), lower lava (Pal, 2011) are product of higher (14–21%) degrees of melting than those that have MORB (or BABB) affinity (3–10%) – sole samples, pillow basalts from South Andaman (Jafri et al., 1990, 2010) and Bompoka Island (Jafri and Sheikh, 2013). Samples from Corbyn's Cove in Pedersen et al. (2010) show a lower degree of melting than those collected in Chidiya Tapu. The one to one correlation of geochemical diversity and degree of mantle melting could be attributed to the two modes of melting - flux induced (higher degree) melting beneath an arc and decompression (lower degree of melting) beneath an extensional setting (e.g. back-arc).

7.2. Contrasting petrological characters of the Andaman ophiolite mantle rocks

Along the stretch of the Andaman islands there is a pronounced variation in terms of petrography and mineral chemistry within the ophiolitic mantle sequence. The restitic peridotite with forearc affinity of Rutland Island is composed of depleted harzburgite to clinopyroxene-bearing harzburgite whereas Middle and North Andaman are dominated by less depleted lherzolite akin to the geochemical signature of abyssal peridotites (Ghosh et al., 2013). The degrees of melting calculated from chrome spinel chemistry indicate low to moderate values (2–10%) for North and Middle Andaman samples, and high values (14–18%) for Rutland peridotites (Ghosh et al., 2018), which corroborate well the degree of melting calculated for the volcanic rocks (pale green and purple boxes in Fig. 9a). Less incompatible trace elements in clinopyroxenes, HREEs in particular, serve as an important proxy for the extent of partial melting since the mineral contains >85% of the trace element budget of the peridotites (Warren et al., 2009). Keeping this in mind, we compare our numerical melting results with the Andaman peridotite clinopyroxene data from Ghosh et al. (2018) (Fig. 9b,c). The chondrite REE spidergram (Fig. 9c) indicates 3–10% melting of DMM for the North and Middle Andaman peridotites and ~ 14% melting for peridotites of Rutland Island, which is in accord with the conclusions of Ghosh et al. (2018). Similar inferences may be drawn from the primitive mantle normalized spidergram (Fig. 9b), especially comparing the HREE pattern.

We have compiled and plotted clinopyroxene compositions of peridotites of the Southern Mariana forearc (Supplementary Fig. 3.a,e; Chen and Zeng, 2007), Izu-Bonin-Mariana forearc (Supplementary Fig. 3.b,f; Parkinson and Pearce, 1998), Tonga forearc (Supplementary Fig. 3c,g; Birner et al., 2017) and supra-subduction zone (SSZ) peridotites from ophiolite complexes of SW Turkey (Supplementary Fig. 3.d,h; Aldanmaz, 2012) to compare them with peridotites from Rutland Island. In case of the Southern Mariana forearc mantle Chen and Zeng (2007) inferred that highly refractory harzburgites are a product of subduction-related mantle metasomatism via hydrous melt. Parkinson and Pearce (1998) interpreted Izu-Bonin forearc peridotites as a result of interaction of a harzburgitic residue with an oxidized boninitic melt in an SSZ setting. However, reassessment of Birner et al. (2017) suggests that enrichments in LREE in the samples could be better explained by disequilibrium melting than by melt addition (interaction with boninitic melt). For Tonga forearc peridotites, two distinct groups have been identified by Birner et al. (2017) based on spinel Cr#, fO_2, and trace element concentrations. Group I is interpreted as residues of large degrees of fractional melting, with minor influence from arc-like melts or fluids, formed during the first stages of subduction initiation whereas Group II is inferred to have formed during flux melting of fertile mantle owing to interaction with subduction-related fluids and/or melts. We find a good match with HREEs of all the above mentioned forearc (SZZ influenced) peridotites, except Group II of the Tonga forearc peridotites. We would also like to point out the close resemblance of Rutland samples with the recently recovered peridotite fragments from Daito Ridge, which is interpreted to be the mantle section of a remnant proto-Philippine Sea island arc (Supplementary Fig. 3i,j; Morishita et al., 2018b). The clinopyroxene compositions of compiled forearc peridotites are shown for reference in Supplementary Fig. 3i,j and also in Fig. 9b,c. Owing to the lack of LREE data of the Rutland peridotites we could not satisfactorily compare the behaviour of such elements. We note one major difference in the primitive mantle normalized multielement pattern from the results of melting experiments, i.e. the enrichment of Nb with respect to Ce in the peridotite samples (Fig. 9b). This behaviour is very prominent in Rutland samples; also, in Tonga Group I peridotites (Supplementary Fig. 3c,g) and Daito Ridge peridotites (Supplementary Fig. 3i,j). Such Nb enrichment could have resulted from the melt mantle interaction in the upper mantle beneath the subduction zone (Kelemen et al., 1993; Stolz et al., 1996). This line of evidence thus confirms the refractory nature of the Rutland peridotite to have formed in a subduction influenced (arc/forearc) environment as suggested by Ghosh et al. (2013, 2018). Further, we can conclude that peridotites like Tonga forearc Group II, which are indicative of a flux melting dominated mature stages of subduction, were either not formed, or are not exposed in the Andaman ophiolite. Ghosh et al. (2018) also documented a close resemblance of the North and Middle Andaman peridotite data with back-arc basin peridotite data from the Mariana Trough (Ohara et al., 2002) and Parece Vela back-arc basin (Ohara et al., 2003), and assigned a back-arc origin to them (shown in Fig. 9b,c). Morishita et al. (2018a) also interpreted the peridotites of Middle Andaman to be the result of low-degree of partial melting with minor flux infiltration, which is likely to take place in a back-arc region. González-Jiménez et al. (2020) recently estimated the parental melt composition for the chromitite pods hosted within the North Andaman lherzolites, which is found to be similar to high-Mg island arc tholeiite (IAT) and boninites (; and broadly analogous with the parental melt of chromitites from Rutland Island that inferred to be formed at supra-subduction zone setting (Ghosh et al., 2009). The back-arc geochemical signature of the lherzolitic peridotites (Ghosh et al., 2018), coupled with the commonly believed melt-mantle interaction origin for podiform chromitites (Arai, 1997; Zhou et al., 1994), thus suggest that the North Andaman lherzolites, after having formed in the back-arc setting, must have been located in the forearc region, where they interacted with arc affinity melt and eventually formed chromitite pods.

7.3. Cretaceous geodynamic evolution of the Sunda subduction zone

Reviewing the previous geochemical and geochronological investigation, Ghosh et al. (2017) explained the formation of the Andaman ophiolite entirely within the context of a single progressive subduction system. However, as pointed out by Bandyopadhyay et al. (2020), this does not adequately explain all our field observations and geochronological constraints. For instance, the 93–95 Ma U-Pb ages for the

plagiogranites of South Andaman were inferred to date ophiolite spreading and subduction initiation (Pedersen et al., 2010). Howeever, the 93.6 Ma (Sarma et al., 2010) plagiogranite-diorite suite from location 3 (Bedonabad coast, South Andaman) has an arc affinity, implying subduction maturation, and has been proposed to be genetically linked with the East Coast volcanics (Jafri et al., 1995). So, the meaning of this 93–95 Ma age is intriguing. The problem becomes obvious when compared with the age of ~106 Ma estimated from plagioclase xenocryst within recently erupted Barren Island volcanic rock (Ray et al., 2015) and the 105–106 Ma cooling age from Andaman ophiolite metamorphic sole (Plunder et al., 2020).

Kinematic restoration of the Andaman Sea back to pre-Oligocene time shifts the Andaman ophiolites to the forearc of Sumatra, immediately west of the Cretaceous Woyla Arc (Advokaat et al., 2018; van Hinsbergen et al., 2011), which collided with and accreted to West Sumatra in the mid Cretaceous (Barber et al., 2005). It has been speculated that this collision supposedly flipped subduction polarity (Advokaat et al., 2018; Plunder et al., 2020). We now integrate field observations and geochemical and geochronological data from the Andaman Ophiolites to test whether the previously speculated polarity reversal could be a possible option to initiate the Sunda subduction system in the west of Sumatra during the Cretaceous.

7.3.1. 99–93 Ma arc magmatism

Here, we interpret the age of 98.5 Ma of the younger zircon in layered gabbro (SA-GAB1) from the nearby location (location 2; Kodiaghat section, South Andaman) as dating the emplacement (Figs. 7,10). These gabbros are interpreted to be genetically linked with the Moho transition zone rocks (olivine-rich troctolite, and clinopyroxenite-wehrlite) at the same location. Olivine-rich troctolite is interpretated to have an origin by impregnation of hydrous basaltic melt into a dunite (replacive) protolith that formed earlier by melt-mantle interaction (Ghosh et al., 2014). The composition of chrome spinels from this olivine-rich troctolite shows a clear affinity to the harzburgitic peridotites of Rutland Island (Ghosh et al., 2014). These peridotites possess forearc geochemical affinity (Ghosh et al., 2013) and are found to have suffered relatively higher degree (~14%) of melting (Fig. 9; Ghosh et al., 2018). The extent of melting that the Rutland peridotites suffered is in concurrence with the degree of melting determined for the East Coast volcanics (Fig. 9a). Ghosh et al. (2014) also showed that melt compositions in equilibrium with clinopyroxene from olivine-rich troctolites and gabbroic rocks fit with the East Coast volcanics. Now we have also found the East Coast volcanics data (Ghosh et al., 2014) to have an arc affinity (Fig. 8). In addition, plagiogranite (148A) from Rutland Island (location 4) gives a 98.7 Ma U/Pb age (Fig. 7). So, arc lithosphere with volcanic rocks (East Coast volcanics), plagiogranite, layered gabbro, lower crustal cumulate and harzburgite had been formed at least by ~99 Ma. Specifically, lithotypes exposed in Bedonabad coast, South Andaman (location 3), thus appear to have formed in an arc setting, where pre-existing gabbroic crust was intruded by arc volcanics and plagiogranites around 93 Ma (Jafri et al., 1995; Sarma et al., 2010). Jafri et al. (1995) presumed that the Andaman plagiogranite, may not be a part of the Andaman ophiolite sequence and may postdate emplacement of the Andaman ophiolite gabbro. Our new geochronological and geochemical results are in accord with this inference.

Agglomerates from Panchawati coast, Middle Andaman (Location 1) and Chidiya Tapu coast, South Andaman (Location 6) unequivocally show arc characteristics (Fig. 8). Interestingly, agglomerates from Chidiya Tapu coast, South Andaman (Location 1) are found to host plagiogranite blocks that presumably have the same age (i.e. 95 ± 2 Ma) as the trondhjemite sample dated by Pedersen et al. (2010) from the same location. Thus agglomerates would have formed during an explosive arc volcanism not earlier than ~95 Ma. The likely cogenetic leucocratic rock L-18 (belonging to the diorite – granodiorite series), associated with Middle Andaman agglomerates, yields a ~ 93.5 Ma age (Fig. 7). Late Cretaceous explosive arc volcanism has been also predicted from the presence of ash layers within the radiolarian cherts in South Andaman (Jafri et al., 2006). Accordingly, based on our results from Middle Andaman, South Andaman and Rutland Island, we postulate that the bulk of magmatic rocks, including gabbros, plagiogranites, and agglomerates found on the Andaman Islands formed in a volcanic arc that had developed by 98–99 Ma and remained active until at least ~93 Ma (Fig. 10).

For supra subduction zone magmatism, a tendency of increasing alkalinity away from the trench has been documented (Wilson, 1989, and references therein) and is thought to reflect cooling of the mantle wedge and the progressive deepening of the melting upon maturation of subduction (Stern et al., 2012; Whattam and Stern, 2011). Thus, the process is expected to yield tholeiitic volcanics in the forearc during subduction zone infancy, followed by gradually more calc-alkaline volcanics. We have tested the alkalinity in the volcanic samples of the Andaman ophiolite with major element based AFM (Irvine and Baragar, 1971) and trace element-based (Ross and Bédard, 2009) discrimination diagrams (Supplementary Fig. 4) and found that the subduction influenced volcanic rocks mostly plot in the tholeiitic to transitional domain with few in calc-alkaline field. This might suggest that agglomerates of South and Middle Andaman were erupted not very far from the trench in the early stages of arc maturation.

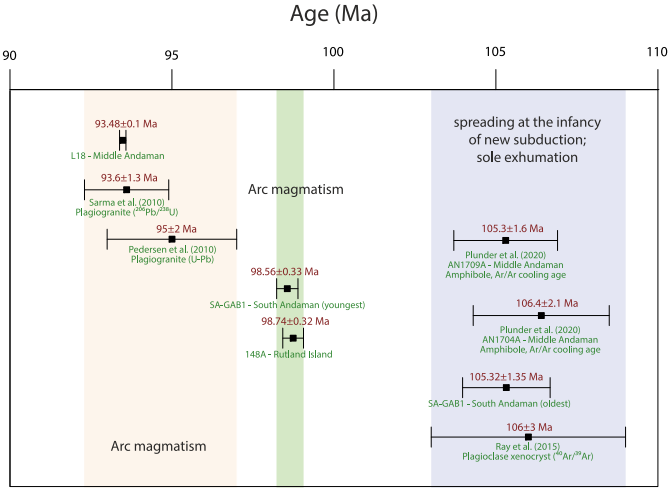

Fig. 10. Geochronological summary of U–Pb zircon ages of magmatic rocks along with Ar–Ar ages from metamorphic sole (Plunder et al., 2020) of Andaman ophiolite; Ar–Ar age from plagioclase xenocryst hosted in Barren lava (Ray et al., 2015) is also shown for reference.

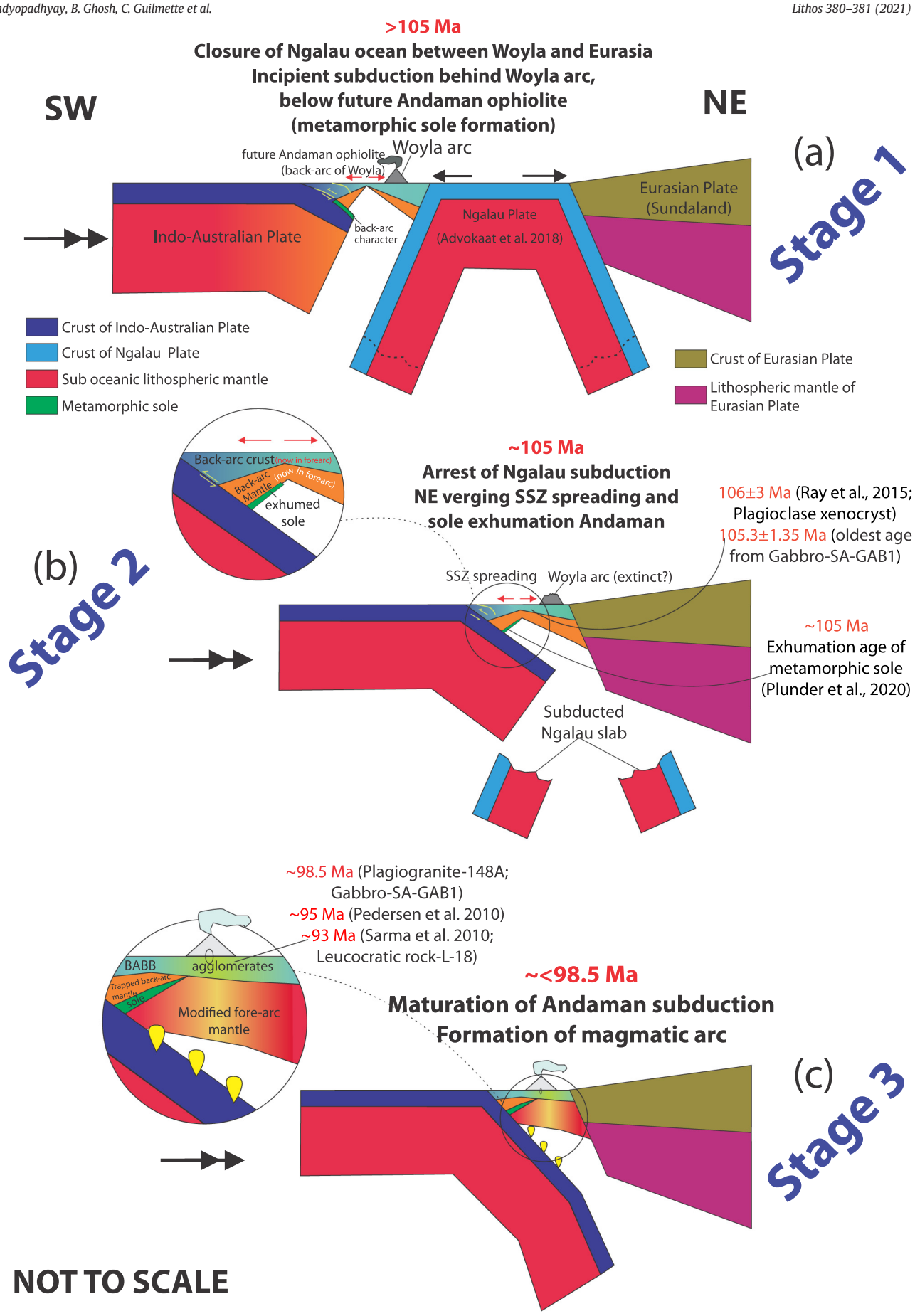

Fig. 11. Schematic reconstruction of Cretaceous subduction initiation and evolution of Andaman ophiolite (see text for details).

7.3.2. Subduction initiation at or before 105 Ma

Though arc characteristics are preserved in most of the crustal rocks (except pillow basalts) and also in Rutland peridotites, the geochemical signatures of Middle Andaman peridotites do not comply with this feature. Ghosh et al. (2013) reported less depleted lherzolitic mantle from Middle Andaman that shows geochemical signatures of abyssal peridotite. These peridotites have been estimated to have suffered relatively low degrees (3–10%) of melting compared to the Rutland peridotites (Ghosh et al., 2018; Fig. 9). The geochemistry of the Middle Andaman peridotites is better explained by depletion in a back-arc setting (Fig. 9b,c; Ghosh et al., 2018). The magmatic precursor rocks of the sole appear to be the product of ~7% mantle melting, which fits well within the estimated extent of melting for the Middle Andaman peridotites below which the sole rocks accreted (see Plunder et al., 2020). Geochemically, metamorphic sole amphibolites (reported by Plunder et al., 2020) also show slab-distal, back-arc basin signatures, with the exception of sample AN1704a (Fig. 8) that yielded an arc signature. In summary, metamorphic sole rocks (originally part of the nascent downgoing slab) and nearby mantle rocks (of the upper plate) (Fig. 1c) both possess back-arc characteristics (Figs. 8,9). This suggests that subduction may have started in a back-arc basin, but not far from the arc. Here, we would like to focus on the $^{40}Ar/^{39}Ar$ ages of 106.4 ± 2.1 Ma and 105.3 ± 1.6 Ma from two amphibolite samples of the metamorphic sole of Middle Andaman (Plunder et al., 2020). Typically, the $^{40}Ar/^{39}Ar$ cooling ages of metamorphic soles coincide with the timing of spreading of SSZ ophiolites, which may suggest that this spreading caused the exhumation of the underlying sole (van Hinsbergen et al., 2015, and references therein). The inherited U/Pb age (~105 Ma) found in one of our magmatic samples (SA-GAB1) suggests crystallization of magmatic zircon at this time, as does the ~106 Ma age found in a xenocrystic plagioclase feldspar in a recent Barren Island volcanic rock (Ray et al., 2015). It has long been thought that $^{40}Ar/^{39}Ar$ ages reflect metamorphic sole formation, and that this in combination with synchronous SSZ spreading marks the timing of subduction initiation (e.g. Maffione et al., 2015; Stern and Bloomer, 1992; Whattam and Stern, 2011). However, recent dating of garnet growth within metamorphic soles of Oman and Turkey with Lu/Hf geochronology has shown that sole growth may predate sole cooling and SSZ ophiolite spreading by >10 Myr (Guilmette et al., 2018; Pourteau et al., 2019). From these arguments, in combination with field observation, geochemical evidences and geochronological constraints we conclude that in the Andaman region subduction initiated at or before 105–106 Ma, in an oceanic back-arc basin environment (Fig. 11). We again emphasize that the cooling age of metamorphic sole, the inherited age of a plagioclase feldspar xenocryst and the inherited U–Pb age of gabbro are closely bracketed within 105–106 Ma, thus reflecting only a minimum age of subduction initiation. The 99–93 Ma arc magmatic rocks thus post-date sole exhumation, and by inference SSZ ophiolite spreading, by 7–13 Myr (Fig. 10), a time delay between SSZ spreading and arc maturation similar to the well-documented case of the Izu-Bonin-Mariana subduction zone (Stern et al., 2012).

7.3.3. Matching the geochemistry with tectonic evolution

Following the above discussion, we here try to assess the tectonic reconstruction reversal, which is suggested to have initiated new subduction in the region (Advokaat et al., 2018; Plunder et al., 2020). Further we will also attempt to reconstruct the stage-wise subduction evolution in Andaman in the regional geodynamic context (Fig. 11).

7.3.3.1. Stage 1 (before 105 Ma, Fig. 11a). From the regional geodynamic perspective, formation of the Woyla Arc has been suggested to be due to westward subduction that occurred simultaneously with (north)eastward subduction below Sundaland (Eurasian plate) from ~130 to ~100–90 Ma (Advokaat et al., 2018; Barber et al., 2005). From plate kinematic and paleomagnetic analyses, Advokaat et al. (2018) postulated that a double verging subduction (of the now-subducted 'Ngalau' oceanic plate, of which remnants of Upper Triassic limestone (Wajzer et al., 1991) and Triassic and Middle Jurassic radiolarian chert (Barber et al., 2005; McCarthy et al., 2001; Munasri and Putra, 2019) are found in the Ngalau Suture on Sumatra), with two trenches bounding the Woyla Arc and Sundaland, was active in this time period. Collision of the Woyla Arc with Sundaland (Eurasian plate) led to southward migration of the trench-trench-trench triple junction between Woyla, Sundaland, and Ngalau, requiring a subduction polarity reversal to maintain a stable triple junction (Advokaat et al., 2018). This reversal led to subduction initiation in the back-arc behind the Woyla Arc, explaining the geochemical signatures of the metamorphic sole rocks (location 1) and of the Andaman lherzolites.

7.3.3.2. Stage 2 (~105 Ma, Fig. 11b). By 105 Ma, a metamorphic sole had formed and was exhuming, presumably simultaneously with SSZ spreading (Plunder et al., 2020). We interpret synchronous magmatism in the upper plate, suggested by the Barren Island 106 Ma xenocryst and the inherited ~105 Ma zircon age documented in this paper, as the reflection of SSZ ophiolite spreading. During this stage, Woyla Arc-Sundaland continent collision may not have been finalized yet, as in the modern equivalent of such a setting found in Timor and Wetar. There, GPS data (Nugroho et al., 2009) show that approximately 30% of Australia-Banda convergence is still accommodated between Timor and Australia, where the Banda arc has been colliding with Australia since the late Miocene (Audley-Charles et al., 1979; Tate et al., 2014, 2015, 2017), and the remainder of convergence is accommodated by the Wetar back-thrust that has formed within the last few million years at the northern edge of the Banda arc (Breen et al., 1989).

7.3.3.3. Stage 3 (<99–93 Ma, Fig. 11c). Newly formed, NE verging subduction evolved to a more mature stage at around 99 Ma and was characterized by cooling of the mantle wedge and the associated deepening of the melting zone. Our new magmatic U–Pb age data of ~98-99 Ma show that new arc volcanoes formed within 7–13 Myr of sole exhumation. This newly formed explosive arc volcano was active at least until 93 Ma and produced most of the exposed rock types in the Andaman islands.

8. Conclusions

We have performed a geochemical and geochronological analysis of magmatic rocks of the Andaman Ophiolites to evaluate the feasibility of a previously speculated process of subduction initiation via polarity reversal. We find that there are two distinct groups of ophiolitic rocks in the Andaman Island. Mantle peridotites as well as mafic amphibolites of the metamorphic sole below the ophiolite have chemical signatures suggestive of an origin in a back-arc basin. Volcanic agglomerates, including plagiogranite xenoliths, suggest formation in a volcanic arc. New U/Pb ages show that arc magmatism occurred between ~99 and 93 Ma, at least 7 Myr later than the cooling of the sub-ophiolitic metamorphic sole that gave ~106–105 Ma hornblende $^{40}Ar/^{39}Ar$ ages. The origin of pillow lava sequences remains ambiguous due to the lack of age constraints and it is a topic of future research. However, their MORB geochemical affinity, with a speculated back-arc basin (slab distal) origin, may suggest that they could have originated at any stages of subduction, where ocean floor spreading was taking place with no or little influence from slab.

We interpret the geochemistry of the Andaman Islands as follows: Restoring the Andaman ophiolites back to the Early Oligocene onset of opening of the Andaman Sea basin brings the ophiolites to the west of the Woyla Arc. The latter had collided with Sumatra around 105–95 Ma. We find that the Andaman ophiolites resulted from a subduction polarity reversal behind an arc (the Woyla Arc), after which SSZ spreading around 105 Ma led to metamorphic sole exhumation. By 99–93 Ma a volcanic arc had developed on the Andaman Islands. This proposed mechanism satisfactorily explains the field relationships

of the geochemically incoherent ophiolitic rock record in the Andaman Islands. Such a petrochemical manifestation of subduction polarity reversal in rock records has not been described in detail before.

Supplementary data to this article can be found online at https://doi.org/10.1016/j.lithos.2020.105853.

Declaration of Competing Interest

The authors declare that they have no known competing financial interests or personal relationships that could have appeared to influence the work reported in this paper.

Acknowledgments

This work is part of the doctoral research (PhD) program of the first author, supported with Department of Science and Technology (DST) INSPIRE Fellowship (IF 130148). D.B specially acknowledges the help received from Dr. Jun-Ichi Kimura (JAMSTEC, Japan) regarding PRIMACALC2 calculation. B.G. acknowledges financial support received from Science and Engineering Research Board, DST, India (EMR/2017/000929). D.J.J.v.H., A.P., and E.L.A. were funded through ERC starting grant SINK (306810) to D.J.J.v.H. D.J.J.v.H. acknowledges NWO Vici grant 865.17.001. The authors thank two anonymous reviewers for their insightful comments and suggestions. We also acknowledge Michael Jentzer for his comments on an earlier version of the manuscript. Editorial handling by Greg Shellnutt is greatly acknowledged. We thank the Ramakrishna mission in Port-Blair for accommodation and Yael Engbers for help during the fieldwork. All data including supporting information for this manuscript are available at Figshare https://doi.org/10.6084/m9.figshare.11396469.v7.

References

Acharyya, S.K., 2007. Collisional emplacement history of the Naga-Andaman ophiolites and the position of the eastern Indian suture. J. Asian Earth Sci. 29, 229–242.

Acharyya, S.K., Ray, K.K., Sengupta, S., 1990. Tectonics of the ophiolite belt from Naga Hills and Andaman Islands, India. Proceed. Indian Acad. Sci.-Earth Planet. Sci. 99, 99–187.

Advokaat, E.L., Bongers, M.L.M., Rudyawan, A., BouDagher-Fadel, M.K., Langereis, C.G., van Hinsbergen, D.J.J., 2018. Early cretaceous origin of the Woyla Arc (Sumatra, Indonesia) on the Australian plate. Earth Planet. Sci. Lett. 498, 348–361.

Agard, P., Yamato, P., Soret, M., Prigent, C., Guillot, S., Plunder, A., Dubacq, B., Chauvet, A., Monié, P., 2016. Plate interface rheological switches during subduction infancy: Control on slab penetration and metamorphic sole formation. Earth Planet. Sci. Lett. 451, 208–220.

Aitchison, J.C., Ao, A., Bhowmik, S., Clarke, G.L., Ireland, T.R., Kachovich, S., Lokho, K., Stojanovic, D., Roeder, T., Truscott, N., Zhen, Y., Zhou, R., 2019. Tectonic evolution of the western margin of the Burma microplate based on new fossil and radiometric age constraints. Tectonics 38, 1718–1741.

Aldanmaz, E., 2012. Trace element geochemistry of primary mantle minerals in spinel-peridotites from polygenetic MOR–SSZ suites of SW Turkey: constraints from an LA-ICP-MS study and implications for mantle metasomatism. Geol. J. 47, 59–76.

Andreason, M.W., Mudford, B., Onge, J.E.S., 1997. Geologic evolution and petroleum system of the Thailand Andaman Sea Basins. Proceedings of an International Conference on Petroleum Systems of SE Asia and Australasia, Indonesian Petroleum Association, pp. 337–350.

Anonymous, 1972. Penrose field conference on ophiolites. Geotimes 17, 24–25.

Arai, S., 1997. Origin of podiform chromitites. J. Asian Earth Sci. 15, 303–310.

Ariskin, A., Barmina, G., 2004. COMAGMAT: development of a magma crystallization model and its petrological applications. Geochem. Int. 42, S1–S157.

Asimow, P.D., Dixon, J.E., Langmuir, C.H., 2004. A hydrous melting and fractionation model for mid-ocean ridge basalts: application to the Mid-Atlantic Ridge near the Azores. Geochem. Geophys. Geosyst. 5.

Audley-Charles, M.G., Carter, D.J., Barber, A.J., Norvick, M.S., Tjokrosapoetro, S., 1979. Reinterpretation of the geology of Seram: implications for the Banda Arcs and northern Australia. J. Geol. Soc. Lond. 136, 547–566.

Awasthi, N., 2017. Provenance and paleo–weathering of Tertiary accretionary prism–forearc sedimentary deposits of the Andaman Archipelago, India. J. Asian Earth Sci. 150, 45–62.

Bandopadhyay, P.C., 2012. Re-interpretation of the age and environment of deposition of Paleogene turbidites in the Andaman and Nicobar Islands, Western Sunda Arc. J. Asian Earth Sci. 45, 126–137.

Bandopadhyay, P.C., 2017. Introduction and history of mapping and research. In: Bandopadhyay, P.C., Carter, A. (Eds.), The Andaman–Nicobar Accretionary Ridge: Geology. Tectonics and Hazards, Geological Society, London, Memoirs vol. 47, pp. 1–7.

Bandopadhyay, P.C., Carter, A., 2017. Mithakhari deposits. In: Bandopadhyay, P.C., Carter, A. (Eds.), The Andaman–Nicobar Accretionary Ridge: Geology. Tectonics and Hazards, Geological Society, London, Memoirs vol. 47, pp. 111–132.

Bandyopadhyay, D., van Hinsbergen, D.J.J., Plunder, A., Bandopadhyay, P.C., Advokaat, E., Chattopadhaya, S., Morishita, T., Ghosh, B., 2020. Andaman Ophiolite: An overview. In: Ray, J.S., Radhakrishna, M. (Eds.), The Andaman Islands and Adjoining Offshore: Geology. Tectonics and Palaeoclimate. Springer International Publishing, Cham, pp. 1–17.

Barber, A.J., 2000. The origin of the Woyla Terranes in Sumatra and the late Mesozoic evolution of the Sundaland margin. J. Asian Earth Sci. 18, 713–738.

Barber, A.J., Crow, M.J., Milsom, J.S., 2005. Sumatra: Geology. Resources and Tectonic Evolution, Geological Society of London.

Bhattacharya, A., Pal, T., Ghosh, B., 2013. Characterization of the accreted ophiolite slices of Rutland Island, Andaman Sea: evolution in a suprasubduction zone setting. Ofioliti 38, 121–142.

Bhattacharya, S., Pande, K., Kumar, A., Kingson, O., Ray, J.S., 2020. Timing of Formation and Obduction of the Andaman Ophiolite. In: Ray, J.S., Radhakrishna, M. (Eds.), The Andaman Islands and Adjoining Offshore: Geology, Tectonics and Palaeoclimate. Springer International Publishing, Cham, pp. 19–42.

Birner, S.K., Warren, J.M., Cottrell, E., Davis, F.A., Kelley, K.A., Falloon, T.J., 2017. Forearc peridotites from tonga record heterogeneous oxidation of the mantle following subduction initiation. J. Petrol. 58, 1755–1780.

Breen, N.A., Silver, E.A., Roof, S., 1989. The Wetar Back Arc thrust belt, eastern Indonesia: the effect of accretion against an irregularly shaped arc. Tectonics 8, 85–98.

Cann, J.R., 1970. Rb, Sr, Y, Zr and Nb in some ocean floor basaltic rocks. Earth Planet. Sci. Lett. 10, 7–11.

Chen, J., Zeng, Z., 2007. Metasomatism of the peridotites from southern Mariana fore-arc: trace element characteristics of clinopyroxene and amphibole. Sci. China Ser. D Earth Sci. 50, 1005–1012.

Corfu, F., 2004. U–Pb Age, setting and Tectonic significance of the Anorthosite–Mangerite–Charnockite–Granite Suite, Lofoten–Vesterålen, Norway. J. Petrol. 45, 1799–1819.

Curray, J.R., 1989. The Sunda Arc: a model for oblique plate convergence. Neth. J. Sea Res. 24, 131–140.

Curray, J.R., 2005. Tectonics and history of the Andaman sea region. J. Asian Earth Sci. 25, 187–232.

Curray, J.R., Moore, D.G., Lawver, L.A., Emmel, F.J., Raitt, R.W., Henry, M., Kieckhefer, R., 1979. Tectonics of the Andaman Sea and Burma. In: Watkins, J.S., Montadert, L., Dickerson, P.W. (Eds.), Geological and Geophysical Investigations of Continental Margins, AAPG Memoir 29. American Association of Petroleum Geologists, pp. 189–198.

Dewey, J.F., 1976. Ophiolite obduction. Tectonophysics 31, 93–120.

Dewey, J.F., Casey, J.F., 2013. The sole of an Ophiolite: the Ordovician Bay of Islands complex, Newfoundland. J. Geol. Soc. Lond. 170, 715–722.

Dilek, Y., Furnes, H., 2011. Ophiolite genesis and global tectonics: geochemical and tectonic fingerprinting of ancient oceanic lithosphere. Geol. Soc. Am. Bull. 123, 387–411.

Dilek, Y., Furnes, H., 2014. Ophiolites and their origins. Elements 10, 93–100.

Floyd, P.A., Winchester, J.A., 1975. Magma type and tectonic setting discrimination using immobile elements. Earth Planet. Sci. Lett. 27, 211–218.

Floyd, P.A., Kelling, G., Gökçen, S.L., Gökçen, N., 1991. Geochemistry and tectonic environment of basaltic rocks from the Misis ophiolitic mélange, South Turkey. Chem. Geol. 89, 263–280.

Frerichs, W.E., 1967. Distribution and ecology of foraminifera in the sediments of the Andaman Sea. University of Southern California Los Angeles, California, p. 282.

Ghiorso, M.S., Hirschmann, M.M., Reiners, P.W., Kress III, V.C., 2002. The pMELTS: a revision of MELTS for improved calculation of phase relations and major element partitioning related to partial melting of the mantle to 3 GPa. Geochem. Geophys. Geosyst. 3, 1–35.

Ghosh, B., Bhatta, K., 2014. Podiform chromitites in lherzolitic mantle rocks (Andaman ophiolite, India): the role of magma/rock interaction and parental melt composition. Bull. Soc. Géol. France 185, 123–130.

Ghosh, B., Pal, T., Bhattacharya, A., Das, D., 2009. Petrogenetic implications of ophiolitic chromite from Rutland Island, Andaman—a boninitic parentage in supra-subduction setting. Mineral. Petrol. 96, 59.

Ghosh, B., Morishita, T., Bhatta, K., 2013. Significance of chromian spinels from the mantle sequence of the Andaman Ophiolite, India: paleogeodynamic implications. Lithos 164-167, 86–96.

Ghosh, B., Morishita, T., Gupta, B.S., Tamura, A., Arai, S., Bandyopadhyay, D., 2014. Moho transition zone in the Cretaceous Andaman ophiolite, India: a passage from the mantle to the crust. Lithos 198, 117–128.

Ghosh, B., Bandyopadhyay, D., Morishita, T., 2017. Andaman–Nicobar Ophiolites, India: Origin, evolution and emplacement. In: Bandopadhyay, P.C., Carter, A. (Eds.), The Andaman–Nicobar Accretionary Ridge: Geology, Tectonics and Hazards 47. Geological Society, London, Memoirs, pp. 95–110.

Ghosh, B., Mukhopadhyay, S., Morishita, T., Tamura, A., Arai, S., Bandyopadhyay, D., Chattopadhaya, S., Ovung, T.N., 2018. Diversity and evolution of suboceanic mantle: constraints from Neotethyan ophiolites at the eastern margin of the Indian plate. J. Asian Earth Sci. 160, 67–77.

González-Jiménez, J.M., Mondal, S.K., Ghosh, B., Griffin, W.L., O'Reilly, S.Y., 2020. Re-Os isotope systematics of sulfides in chromitites and host lherzolites of the Andaman Ophiolite, India. Minerals 10, 686.

Guilmette, C., Hébert, R., Dupuis, C., Wang, C., Li, Z., 2008. Metamorphic history and geodynamic significance of high-grade metabasites from the ophiolitic mélange beneath the Yarlung Zangbo ophiolites, Xigaze area, Tibet. J. Asian Earth Sci. 32, 423–437.

Guilmette, C., Hébert, R., Wang, C., Villeneuve, M., 2009. Geochemistry and geochronology of the metamorphic sole underlying the Xigaze Ophiolite, Yarlung Zangbo Suture Zone, South Tibet. Lithos 112, 149–162.
Guilmette, C., Hébert, R., Dostal, J., Indares, A., Ullrich, T., Bédard, É., Wang, C., 2012. Discovery of a dismembered metamorphic sole in the Saga ophiolitic mélange, South Tibet: assessing an early cretaceous disruption of the Neo-Tethyan supra-subduction zone and consequences on basin closing. Gondwana Res. 22, 398–414.
Guilmette, C., Smit, M.A., van Hinsbergen, D.J.J., Gürer, D., Corfu, F., Charette, B., Maffione, M., Rabeau, O., Savard, D., 2018. Forced subduction initiation recorded in the sole and crust of the Semail Ophiolite of Oman. Nat. Geosci. 11, 688–695.
Hacker, B.R., Gnos, E., 1997. The conundrum of Samail: explaining the metamorphic history. Tectonophysics 279, 215–226.
Herzberg, C., Asimow, P.D., 2008. Petrology of some oceanic island basalts: PRIMELT2.XLS software for primary magma calculation. Geochem. Geophys. Geosyst. 9.
van Hinsbergen, D.J.J., Kapp, P., Dupont-Nivet, G., Lippert, P.C., DeCelles, P.G., Torsvik, T.H., 2011. Restoration of Cenozoic deformation in Asia and the size of Greater India. Tectonics 30.
van Hinsbergen, D.J.J., Peters, K., Maffione, M., Spakman, W., Guilmette, C., Thieulot, C., Plümper, O., Gürer, D., Brouwer, F.M., Aldanmaz, E., Kaymakcı, N., 2015. Dynamics of intraoceanic subduction initiation: 2. Suprasubduction zone ophiolite formation and metamorphic sole exhumation in context of absolute plate motions. Geochem. Geophys. Geosyst. 16, 1771–1785.
Hutchison, C.S., 1975. Ophiolite in Southeast Asia. GSA Bull. 86, 797–806.
Imsong, W., Choudhury, S., Phukan, S., 2016. Ascertaining neotectonic activities in the southern part of Shillong Plateau through geomorphic parameters and remote sensing data. Curr. Sci. 110, 91–98.
Irvine, T.N., Baragar, W.R.A., 1971. A guide to the chemical classification of the common volcanic rocks. Can. J. Earth Sci. 8, 523–548.
Ishikawa, T., Fujisawa, S., Nagaishi, K., Masuda, T., 2005. Trace element characteristics of the fluid liberated from amphibolite-facies slab: Inference from the metamorphic sole beneath the Oman ophiolite and implication for boninite genesis. Earth Planet. Sci. Lett. 240, 355–377.
Jaffey, A.H., Flynn, K.F., Glendenin, L.E., Bentley, W.C., Essling, A.M., 1971. Precision measurement of half-lives and specific activities of 235U and 238U. Phys. Rev. C 4, 1889–1906.
Jafri, S.H., 1986. Occurrence of Hagistrids in chert associated with Port Blair Seies, South Andaman, India. J. Geol. Soc. India 28, 41–43.
Jafri, S.H., Sheikh, J.M., 2013. Geochemistry of pillow basalts from Bompoka, Andaman–Nicobar islands, Bay of Bengal, India. J. Asian Earth Sci. 64, 27–37.
Jafri, S.H., Balaram, V., Ramesh, S.L., 1990. Geochemistry of Andaman-Nicobar island basalts: a case for a possible plume origin. J. Volcanol. Geotherm. Res. 44, 339–347.
Jafri, S.H., Balaram, V., Govil, P.K., 1993. Depositional environments of cretaceous radiolarian cherts from Andaman-Nicobar Islands, northeastern Indian Ocean. Mar. Geol. 112, 291–301.
Jafri, S.H., Charan, S.N., Govil, P.K., 1995. Plagiogranite from the Andaman ophiolite belt, Bay of Bengal, India. J. Geol. Soc. Lond. 152, 681–687.
Jafri, S.H., Rao, M.V.S., Ramesh, S.L., 2006. Occurrence of ash beds in radiolarian cherts from South Andaman Island, Bay of Bengal, India: evidence for late cretaceous explosive volcanism. Curr. Sci. 91, 1614–1615.
Jafri, S.H., Sarma, D.S., Sheikh, J.M., 2010. Hyaloclastites in pillow basalts, South Andaman Island, Bay of Bengal, India. Curr. Sci. 99, 1825–1829.
Kamesh Raju, K.A., Ramprasad, T., Rao, P.S., Ramalingeswara Rao, B., Varghese, J., 2004. New insights into the tectonic evolution of the Andaman basin, Northeast Indian Ocean. Earth Planet. Sci. Lett. 221, 145–162.
Kamili, Z.A., Kingston, J., Achmad, Z., Wahab, A., Sosromihardjd, S., Crausaz, C.U., 1976. Contribution to the Pre–Baong Stratigraphy of North Sumatra. 5th annual convention proceedings. Indones. Petrol. Assoc. 2, 91–108.
Karunakaran, C., Pawde, M.B., Raina, V.K., Ray, K.K., 1964. Geology of the South Andaman Island, India, Reports 22nd International Geological Congress. New Delhi, India XI, pp. 79–100.
Kelemen, P.B., Shimizu, N., Dunn, T., 1993. Relative depletion of niobium in some arc magmas and the continental crust: partitioning of K, Nb, La and Ce during melt/rock reaction in the upper mantle. Earth Planet. Sci. Lett. 120, 111–134.
Kempton, P.D., Harmon, R.S., 1992. Oxygen isotope evidence for large-scale hybridization of the lower crust during magmatic underplating. Geochim. Cosmochim. Acta 56, 971–986.
Kimura, J.-I., Ariskin, A.A., 2014. Calculation of water-bearing primary basalt and estimation of source mantle conditions beneath arcs: PRIMACALC2 model for WINDOWS. Geochem. Geophys. Geosyst. 15, 1494–1514.
Krogh, T.E., 1973. A low-contamination method for hydrothermal decomposition of zircon and extraction of U and Pb for isotopic age determinations. Geochim. Cosmochim. Acta 37, 485–494.
Lay, T., Kanamori, H., Ammon, C.J., Nettles, M., Ward, S.N., Aster, R.C., Beck, S.L., Bilek, S.L., Brudzinski, M.R., Butler, R., DeShon, H.R., Ekström, G., Satake, K., Sipkin, S., 2005. The Great Sumatra-Andaman earthquake of 26 December 2004. Science 308, 1127–1133.
Le Bas, M.J., Le Maitre, R.W., Streckeisen, A., Zanettin, B., IUGS Subcommission on the Systematics of Igneous Rocks, 1986. A chemical classification of volcanic rocks based on the total alkali-silica diagram. J. Petrol. 27, 745–750.
Ling, H.Y., Chandra, R., Karkare, S.G., 1996. Tectonic significance of Eocene and Cretaceous radiolaria from South Andaman Island, northeast Indian Ocean. Island Arc 5, 166–179.
Ling, H.Y., Srinivasan, M.S., 1993. Significance of Eocene Radiolaria from Port Blair Group of South Andaman Island, India. J. Palaeontol. Soc. India 38, 1–5.
Ling, H.Y., Sharma, V., Singh, S., Mazumdar, D., Mahapatra, A.K., 1995. Cretaceous and Middle Eocene Radiolaria from Ejected Sediments of mud Volcanoes of Baratang Island in Andaman Sea of the Northeastern Indian Ocean. J. Geol. Soc. India 45, 463–469.
Liu, C.-Z., Chung, S.-L., Wu, F.-Y., Zhang, C., Xu, Y., Wang, J.-G., Chen, Y., Guo, S., 2016a. Tethyan suturing in Southeast Asia: Zircon U-Pb and Hf-O isotopic constraints from Myanmar ophiolites. Geology 44, 311–314.
Liu, C.-Z., Zhang, C., Xu, Y., Wang, J.-G., Chen, Y., Guo, S., Wu, F.-Y., Sein, K., 2016b. Petrology and geochemistry of mantle peridotites from the Kalaymyo and Myitkyina ophiolites (Myanmar): Implications for tectonic settings. Lithos 264, 495–508.
Ludwig, K.R., 2009. Isoplot 4.1. A geochronological toolkit for Microsoft Excel. 4. Berkeley Geochronology Center Special Publication, p. 76.
Maffione, M., Thieulot, C., van Hinsbergen, D.J.J., Morris, A., Plümper, O., Spakman, W., 2015. Dynamics of intraoceanic subduction initiation: 1. Oceanic detachment fault inversion and the formation of supra-subduction zone ophiolites. Geochem. Geophys. Geosyst. 16, 1753–1770.
Mattinson, J.M., 2005. Zircon U–Pb chemical abrasion ("CA-TIMS") method: combined annealing and multi-step partial dissolution analysis for improved precision and accuracy of zircon ages. Chem. Geol. 220, 47–66.
McCarthy, A.J., Jasin, B., Haile, N.S., 2001. Middle Jurassic radiolarian chert, Indarung, Padang District, and its implications for the tectonic evolution of western Sumatra, Indonesia. J. Asian Earth Sci. 19 (1), 31–44.
McDonough, W.F., Sun, S.s., 1995. The composition of the Earth. Chem. Geol. 120, 223–253.
Meltzner, A.J., Sieh, K., Abrams, M., Agnew, D.C., Hudnut, K.W., Avouac, J.-P., Natawidjaja, D.H., 2006. Uplift and subsidence associated with the great Aceh-Andaman earthquake of 2004. J. Geophys. Res. Solid Earth 111, B02407.
Morishita, T., Ghosh, B., 2010. The 26 December 2004 Sumatra-Andaman Tsunami at the South Andaman Island: 5 years later. J. Geol. Soc. Jpn. 116, V–VI.
Morishita, T., Yoshikawa, M., Tamura, A., Guotana, J.M., Ghosh, B., 2018a. Petrology of peridotites and Nd-Sr isotopic composition of their clinopyroxenes from the middle Andaman Ophiolite, India. Minerals 8, 410.
Morishita, T., Tani, K.-I., Soda, Y., Tamura, A., Mizukami, T., Ghosh, B., 2018b. The uppermost mantle section below a remnant proto-Philippine Sea island arc: Insights from the peridotite fragments from the Daito Ridge. Am. Mineral. 103, 1151–1160.
Morley, C.K., Arboit, F., 2019. Dating the onset of motion on the Sagaing fault: evidence from detrital zircon and titanite U-Pb geochronology from the North Minwun Basin, Myanmar. Geology 47, 581–585.
Mukhopadhyay, M., Dasgupta, S., 1988. Deep structure and tectonics of the burmese arc: constraints from earthquake and gravity data. Tectonophysics 149, 299–322.
Munasri, Putra, A.M., 2019. First evidence of Middle to late Triassic radiolarians in the Garba mountains, South Sumatra, Indonesia. Island Arc 28 (3), e12298.
Nugroho, H., Harris, R., Lestariya, A.W., Maruf, B., 2009. Plate boundary reorganization in the active Banda Arc–continent collision: insights from new GPS measurements. Tectonophysics 479, 52–65.
Ohara, Y., Stern, R.J., Ishii, T., Yurimoto, H., Yamazaki, T., 2002. Peridotites from the Mariana trough: first look at the mantle beneath an active back-arc basin. Contrib. Mineral. Petrol. 143, 1–18.
Ohara, Y., Fujioka, K., Ishii, T., Yurimoto, H., 2003. Peridotites and gabbros from the Parece Vela backarc basin: unique tectonic window in an extinct backarc spreading ridge. Geochem. Geophys. Geosyst. 4.
Pal, T., 2011. Petrology and geochemistry of the Andaman ophiolite: melt–rock interaction in a suprasubduction-zone setting. J. Geol. Soc. Lond. 168, 1031–1045.
Pal, T., Bhattacharya, A., 2010. Greenschist-facies sub-ophiolitic metamorphic rocks of Andaman Islands, Burma–Java subduction complex. J. Asian Earth Sci. 39, 804–814.
Pal, T., Bhattacharya, A., 2016. Evolution of Andaman Ophiolite in the Backdrop of Andaman- Java Subduction—A Comprehensive Approach Integrating Field and Laboratory Data. Geological Survey of India Special Publication.
Pal, T., Chakraborty, P.P., Gupta, T.D., Singh, C.D., 2003. Geodynamic evolution of the outer-arc–forearc belt in the Andaman Islands, the central part of the Burma–Java subduction complex. Geol. Mag. 140, 289–307.
Pal, T., Mitra, S.K., Sengupta, S., Katari, A., Bandopadhyay, P.C., Bhattacharya, A.K., 2007. Dacite–andesites of Narcondam volcano in the Andaman Sea — an imprint of magma mixing in the inner arc of the Andaman–Java subduction system. J. Volcanol. Geotherm. Res. 168, 93–113.
Pal, T., Raghav, S., Bhattacharya, A., Bandopadhyay, P.C., Mitra, S.K., Renjit, M.L., Sankar, M.S., Ghosh, B., 2010. The 2005–2006-eruption of the Barren Volcano, Andaman Sea: Evolution of basaltic magmatism in island arc setting of Andaman–Java subduction complex. J. Asian Earth Sci. 39, 12–23.
Parkinson, I.J., Pearce, J.A., 1998. Peridotites from the Izu–Bonin–Mariana Forearc (ODP Leg 125): evidence for Mantle Melting and Melt–mantle interaction in a supra-subduction zone setting. J. Petrol. 39, 1577–1618.
Parlak, O., 2016. The tauride ophiolites of Anatolia (Turkey): a review. J. Earth Sci. 27, 901–934.
Pearce, J.A., 1975. Basalt geochemistry used to investigate past tectonic environments on Cyprus. Tectonophysics 25, 41–67.
Pearce, J.A., 2008. Geochemical fingerprinting of oceanic basalts with applications to ophiolite classification and the search for Archean oceanic crust. Lithos 100, 14–48.
Pearce, J.A., 2014. Immobile element fingerprinting of ophiolites. Elements 10, 101–108.
Pearce, J.A., Cann, J.R., 1971. Ophiolite origin investigated by discriminant analysis using Ti, Zr and Y. Earth Planet. Sci. Lett. 12, 339–349.
Pearce, J.A., Lippard, S.J., Roberts, S., 1984. Characteristics and tectonic significance of supra-subduction zone ophiolites. In: Kokelaar, B.P., Howells, M.F. (Eds.), Marginal Basin Geology: Volcanic and Associated Sedimentary and Tectonic Processes in Modern and Ancient Marginal Basins. 16. Geological Society, London, pp. 77–94 Special Publications.

Pearce, J.A., Dilek, Y., Newcomb, S., 2003. Supra-subduction zone ophiolites: the search for modern analogues. In: Dilek, Y., Newcomb, S. (Eds.), Ophiolite Concept and the Evolution of Geological Thought 373. Geological Society of America, pp. 269–293.
Pedersen, R.B., Searle, M.P., Carter, A., Bandopadhyay, P.C., 2010. U–Pb zircon age of the Andaman ophiolite: implications for the beginning of subduction beneath the Andaman–Sumatra arc. J. Geol. Soc. Lond. 167, 1105–1112.
Plunder, A., Bandyopadhyay, D., Ganerød, M., Advokaat, E.L., Ghosh, B., Bandopadhyay, P., van Hinsbergen, D.J.J., 2020. History of subduction polarity reversal during arc-continent collision: constraints from the Andaman Ophiolite and its metamorphic sole. Tectonics 39 e2019TC005762.
Polachan, S., Racey, A., 1994. Stratigraphy of the Mergui Basin, Andaman Sea: implications for petroleum exploration. J. Pet. Geol. 17, 373–406.
Pourteau, A., Scherer, E.E., Schorn, S., Bast, R., Schmidt, A., Ebert, L., 2019. Thermal evolution of an ancient subduction interface revealed by Lu–Hf garnet geochronology, Halilbağı complex (Anatolia). Geosci. Front. 10, 127–148.
Ray, K.K., 1985. East coast volcanics: a new suite in the ophiolite of Andaman Islands. Records Geol. Surv. India 116, 83–87.
Ray, K.K., Sengupta, S., van Den Hul, H.J., 1988. Chemical characters of volcanic rocks from Andaman ophiolite, India. J. Geol. Soc. Lond. 145, 393–400.
Ray, J.S., Pande, K., Bhutani, R., 2015. 40Ar/39Ar geochronology of subaerial lava flows of Barren Island volcano and the deep crust beneath the Andaman Island Arc, Burma Microplate. Bull. Volcanol. 77, 57.
Reagan, M.K., Ishizuka, O., Stern, R.J., Kelley, K.A., Ohara, Y., Blichert-Toft, J., Bloomer, S.H., Cash, J., Fryer, P., Hanan, B.B., Hickey-Vargas, R., Ishii, T., Kimura, J.-I., Peate, D.W., Rowe, M.C., Woods, M., 2010. Fore-arc basalts and subduction initiation in the Izu-Bonin-Mariana system. Geochem. Geophys. Geosyst. 11.
Rodolfo, K.S., 1969a. Bathymetry and Marine Geology of the Andaman Basin, and tectonic implications for Southeast Asia. GSA Bull. 80, 1203–1230.
Rodolfo, K.S., 1969b. Sediments of the Andaman Basin, northeastern Indian Ocean. Mar. Geol. 7, 371–402.
Ross, P.-S., Bédard, J.H., 2009. Magmatic affinity of modern and ancient subalkaline volcanic rocks determined from trace-element discriminant diagrams. Can. J. Earth Sci. 46, 823–839.
Roy, D.K., Acharyya, S.K., Ray, K.K., Lahiri, T.C., Sen, M.K., 1988. Nature of occurrence and depositional environment of the oceanic pelagic sediments associated with the ophiolite assemblage, South Andaman Island. Indian Minerals 42, 31–56.
Saccani, E., 2015. A new method of discriminating different types of post-Archean ophiolitic basalts and their tectonic significance using Th-Nb and Ce-Dy-Yb systematics. Geosci. Front. 6, 481–501.
Sachin, R., Verma, S., Pal, T., 2017. Petrochemical and petrotectonic characterisation of ophiolitic volcanics from Great Nicobar island Andaman-Sumatra belt. J. Geol. Soc. India 90, 85–92.
Saha, A., Dhang, A., Ray, J., Chakraborty, S., Moecher, D., 2010. Complete preservation of ophiolite suite from south Andaman, India: a mineral-chemical perspective. J. Earth Syst. Sci. 119, 365–381.
Sarma, D.S., Jafri, S.H., Fletcher, I.R., McNaughton, N.J., 2010. Constraints on the tectonic setting of the Andaman Ophiolites, Bay of Bengal, India, from SHRIMP U-Pb zircon geochronology of plagiogranite. J. Geol. 118, 691–697.
Saunders, A., Tarney, J., 1991. Back-arc basins. In: Floyd, P.A. (Ed.), Oceanic Basalts. Springer US, Boston, MA, pp. 219–263.
Schärer, U., 1984. The effect of initial230Th disequilibrium on young U-Pb ages: the Makalu case, Himalaya. Earth Planet. Sci. Lett. 67, 191–204.
Schilling, J.G., Zajac, M., Evans, R., Johnston, T., White, W., Devine, J.D., Kingsley, R., 1983. Petrologic and geochemical variations along the Mid-Atlantic Ridge from 29 degrees N to 73 degrees N. Am. J. Sci. 283, 510–586.
Sengupta, S., Ray, K.K., Acharyya, S.K., de Smeth, J.B., 1990. Nature of ophiolite occurrences along the eastern margin of the Indian plate and their tectonic significance. Geology 18, 439–442.
Shervais, J.W., 1982. Ti-V plots and the petrogenesis of modern and ophiolitic lavas. Earth Planet. Sci. Lett. 59, 101–118.
Shervais, J.W., 2001. Birth, death, and resurrection: the life cycle of suprasubduction zone ophiolites. Geochem. Geophys. Geosyst. 2 2000GC000080.
Sheth, H., 2014. What drives centuries-long polygenetic scoria cone activity at Barren Island volcano? J. Volcanol. Geotherm. Res. 289, 64–80.
Singh, A.K., Chung, S.-L., Bikramaditya, R.K., Lee, H.Y., 2017. New U–Pb zircon ages of plagiogranites from the Nagaland–Manipur Ophiolites, Indo-Myanmar Orogenic Belt, NE India. J. Geol. Soc. Lond. 174, 170–179.
Smith, P.M., Asimow, P.D., 2005. Adiabat_1ph: a new public front-end to the MELTS, pMELTS, and pHMELTS models. Geochem. Geophys. Geosyst. 6 0.1029/2004GC000816.
Soret, M., Agard, P., Dubacq, B., Plunder, A., Yamato, P., 2017. Petrological evidence for stepwise accretion of metamorphic soles during subduction infancy (Semail ophiolite, Oman and UAE). J. Metamorph. Geol. 35, 1051–1080.
Srivastava, R.K., Chandra, R., Shastry, A., 2004. High-Ti type N-MORB parentage of basalts from the south Andaman ophiolite suite, India. J. Earth Syst. Sci. 113, 605–618.
Stacey, J.S., Kramers, J.D., 1975. Approximation of terrestrial lead isotope evolution by a two-stage model. Earth Planet. Sci. Lett. 26, 207–221.
Stern, R.J., Bloomer, S.H., 1992. Subduction zone infancy: examples from the Eocene Izu-Bonin-Mariana and Jurassic California arcs. Geol. Soc. Am. Bull. 104, 1621–1636.
Stern, R.J., Reagan, M., Ishizuka, O., Ohara, Y., Whattam, S., 2012. To understand subduction initiation, study forearc crust: to understand forearc crust, study ophiolites. Lithosphere 4, 469–483.
Stolz, A.J., Jochum, K.P., Spettel, B., Hofmann, A.W., 1996. Fluid- and melt-related enrichment in the subarc mantle: evidence from Nb/Ta variations in island-arc basalts. Geology 24, 587–590.
Sun, S.-S., McDonough, W.F., 1989. Chemical and isotopic systematics of oceanic basalts: implications for mantle composition and processes. In: Saunders, A.D., Norry, M.J. (Eds.), Magmatism in the Ocean Basins. 42. Geological Society, London, pp. 313–345 Special Publications.
Tate, G.W., McQuarrie, N., van Hinsbergen, D.J.J., Bakker, R.R., Harris, R., Willett, S., Reiners, P.W., Fellin, M.G., Ganerød, M., Zachariasse, W.J., 2014. Resolving spatial heterogeneities in exhumation and surface uplift in Timor-Leste: constraints on deformation processes in young orogens. Tectonics 33, 1089–1112.
Tate, G.W., McQuarrie, N., van Hinsbergen, D.J.J., Bakker, R.R., Harris, R., Jiang, H., 2015. Australia going down under: quantifying continental subduction during arc-continent accretion in Timor-Leste. Geosphere 11, 1860–1883.
Tate, G.W., McQuarrie, N., Tiranda, H., van Hinsbergen, D.J.J., Harris, R., Zachariasse, W.J., Fellin, M.G., Reiners, P.W., Willett, S.D., 2017. Reconciling regional continuity with local variability in structure, uplift and exhumation of the Timor orogen. Gondwana Res. 49, 364–386.
Vohra, C.P., Haldar, D., Roy, A.K.G., 1989. The Andaman–Nicobar ophiolite complex and associated mineral resources – current appraisal. In: Ghose, N.C. (Ed.), Phanerozoic Ophiolites of India, pp. 281–315.
Wajzer, M.R., Barber, A.J., Hidayat, S., 1991. Accretion, collision and strike-slip faulting: the Woyla group as a key to the tectonic evolution of North Sumatra. J. SE Asian Earth Sci. 6, 447–461.
Wakabayashi, J., Dilek, Y., 2003. What constitutes 'emplacement' of an ophiolite?: Mechanisms and relationship to subduction initiation and formation of metamorphic soles. In: Dilek, Y., Robinson, P.T. (Eds.), Ophiolites in Earth History. Geological Society, London, Special Publications vol. 218, pp. 427–447.
Warren, J.M., Shimizu, N., Sakaguchi, C., Dick, H.J.B., Nakamura, E., 2009. An assessment of upper mantle heterogeneity based on abyssal peridotite isotopic compositions. J. Geophys. Res.: Solid Eart 114.
Westerweel, J., Roperch, P., Licht, A., Dupont-Nivet, G., Win, Z., Poblete, F., Ruffet, G., Swe, H.H., Thi, M.K., Aung, D.W., 2019. Burma Terrane part of the Trans-Tethyan arc during collision with India according to palaeomagnetic data. Nat. Geosci. 12, 863–868.
Whattam, S.A., Stern, R.J., 2011. The 'subduction initiation rule': a key for linking ophiolites, intra-oceanic forearcs, and subduction initiation. Contrib. Mineral. Petrol. 162, 1031–1045.
Wilson, M., 1989. Chapter 6 - Island Arcs in Igneous Petrogenesis. Igneous Petrogenesis. Springer, Netherlands, pp. 153–190.
Workman, R.K., Hart, S.R., 2005. Major and trace element composition of the depleted MORB mantle (DMM). Earth Planet. Sci. Lett. 231, 53–72.
Zhang, J., Xiao, W., Windley, B.F., Wakabayashi, J., Cai, F., Sein, K., Wu, H., Naing, S., 2018. Multiple alternating forearc-and backarc-ward migration of magmatism in the Indo-Myanmar Orogenic Belt since the Jurassic: documentation of the orogenic architecture of eastern Neotethys in SE Asia. Earth Sci. Rev. 185, 704–731.
Zhou, M.F., Robinson, P.T., Bai, W.J., 1994. Formation of podiform chromitites by melt/rock interaction in the upper mantle. Mineral. Deposita 29, 98–101.